LEVEL

(11)

AD A088331

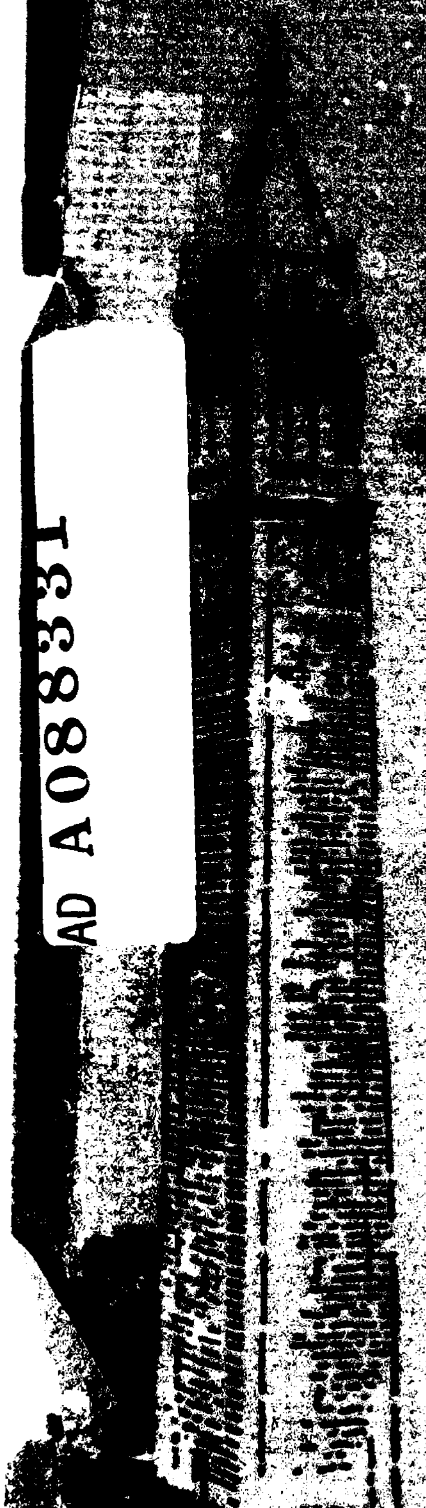

[illegible]

[illegible]

October 1 – December [illegible]

[illegible]

[illegible]

ELECTRONICS [illegible]

College of [illegible]

University of [illegible]

(9) Quarterly progress report
1 Oct-31 Dec 79

(11)

FOURTH QUARTER PROGRESS REPORT

on

(6) PLASMA THEORY and SIMULATION.

(October 1 to December 31, 1979)

F 4-A071758
#18 #3-A071512-79

Research during the Fourth Quarter of 1979 is reported here.

Our research group uses both theory and simulation as tools in order to increase the understanding of instabilities, heating, transport, and other phenomena in plasmas. We also work on the improvement of simulation, both theoretically and practically.

Our staff is (10)

(12) 102

Professor C. K. Birdsall *Principal Investigator*	191 M	Cory Hall	(642-4015)
Alex Friedman *Post Doctorate*	119 ME	Cory Hall	(642-3477)
Bruce Cohen, William Nevins *Lecturers UCB; Physicists LLL*	L439 L439	LLL LLL	(422-9823) (422-7032)
William Fawley *Guest UCB; Physicist LLL*	L321	LLL	(422-9272)
Yu Jiuan Chen, Douglas Harned, Vincent Thomas, Niels Otani *Research Assistants*	119 MD	Cory Hall	(642-1297)
Stephen Au-Yeung *Programmer*	119 MD	Cory Hall	(642-1297)
Mike Hoagland *Research Typist*	199 M	Cory Hall	(642-7919)

(11) 31 Dec [redacted]79

DOE Contract DE-AS03-76F00034-DE-AT03-76ET53064
ONR Contract N00014-77-C-0578.
(15) DE-AS03-76F00034-DE-AT03-76ET53064

ELECTRONICS RESEARCH LABORATORY
College of Engineering
University of California, Berkeley
94720

127550

TABLE OF CONTENTS

*Indicates ONR supported areas.

Section I

PLASMA THEORY and SIMULATION

A. LOWER HYBRID DRIFT INSTABILITY SIMULATIONS USING ES1 HYBRID CODE

Yu-Jiuan Chen (Dr. Bruce Cohen (LLL) and Prof. C. K. Birdsall)

In the last QPR, it was shown that our simulations exhibited strong ion trapping at saturation in the lower-drift-velocity regime with $v_E < v_{ti}$ as our model had assumed a constant density and v_E drift. The typical total ion momentum (Fig. 1a) and ion kinetic energy (Fig. 1b) are exponentially growing in time in the linear regime. In Fig. 1a, the net ion momentum increases in the negative x direction which is the wave propagation direction. Recall that ions in our model are initially in an electrostatic, steady equilibrium state with the ion diamagnetic drift velocity cancelled by the $\underset{\sim}{E} \times \underset{\sim}{B}$ drift velocity, i.e.,

$$v_E = v_{*i} = \frac{T_i}{m_i \omega_{ci}} \left| \frac{d}{dy} \ell n\, n \right| \tag{1}$$

or $v_{di} = v_E - v_{*i} = 0.$, where v_{di} is the ion drift velocity. Also, ions are shielded by the strongly magnetized electrons which are represented by a linear electron susceptibility, $\chi_e(i(\partial/\partial t) - kv_{de},\ v_{*e}(T_e))$, i.e.,

$$\chi_e\left(i \frac{\partial}{\partial t} - kv_{de}, v_{*e}(T_e)\right) k^2 \phi_k = 4\pi \rho_k \tag{2}$$

where $v_{*e} = T_e/m_e\omega_{ce} \left| \frac{d}{dy} \ell n\, n \right|$ is the electron diamagnetic drift and $T_e = m_e v_{te}^2$. v_{de} is the electron drift velocity given by

$$v_{de} = v_E + v_{*e} = v_E(1 + T_e/T_i) \approx v_E \tag{3}$$

as $T_e/T_i \ll 1$.

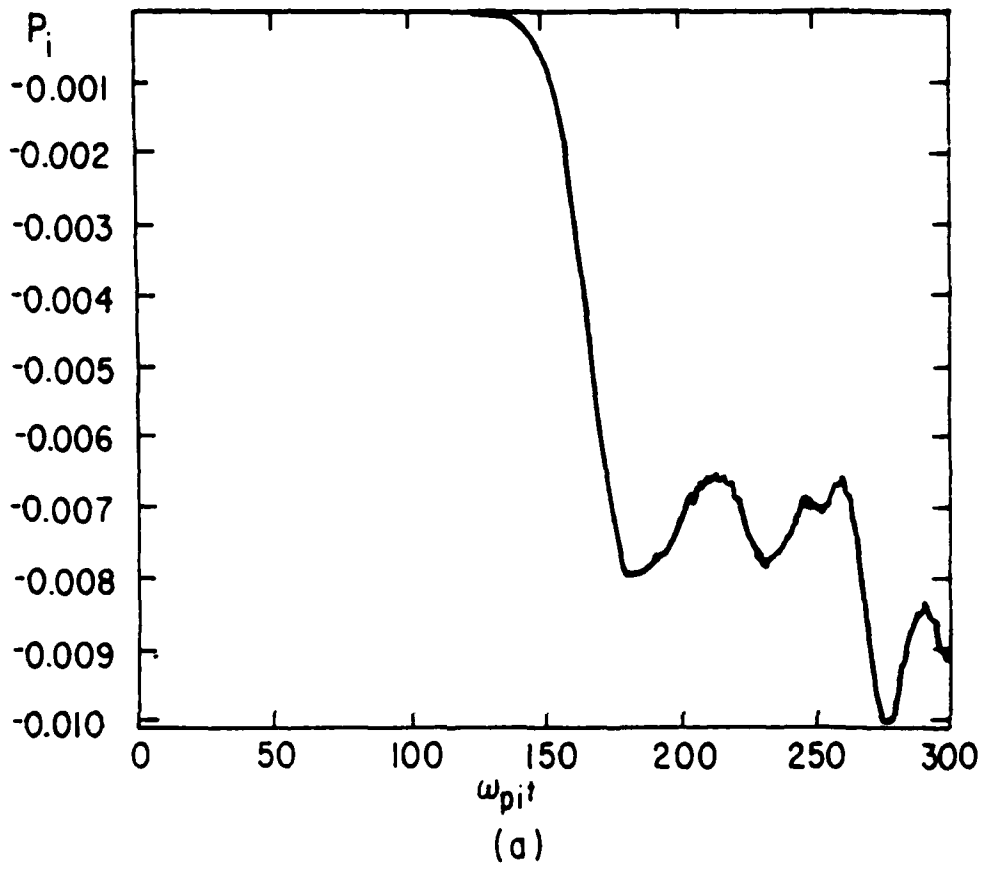

FIG. 1a. History plots of (a) the total ion momentum and ...

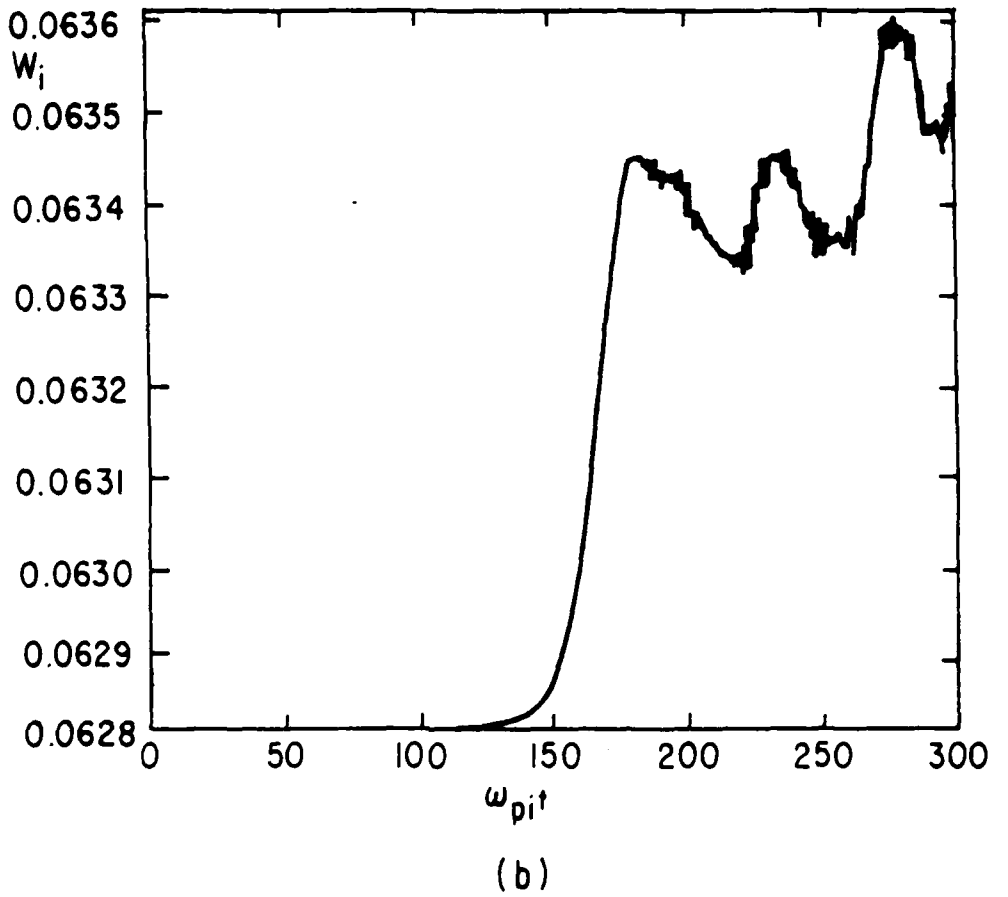

(b)

FIG. 1b. ... (b) kinetic energy for $m_i/m_e = 1600$, $\omega_{pe}^2/\omega_{ce}^2 = 1$, $T_e = 0$, $k\lambda_D = 1/\sqrt{2}$, $L_n/L_B = 0$, $L_n/L_T = 0$, and $v_E/v_{ti} = 0.57$.

From the momentum conservation law,

$$nm_e v_{de}(0) = P_i(t) + nm_e v_{de}(t) - P_i(0) \quad \text{and} \quad P_i(0) = 0 , \quad (4)$$

the increase of ion momentum in the direction of wave propagation implies that current relaxation ($v_d(t) \to 0$) occurs during the growth of the instability, where $v_d = v_{de} - v_{di}$ is the cross-field current velocity or the electron velocity in the ion frame. v_d is no longer constant in time in the late stage of growth. Similarly, it is noted that the electron random kinetic energy must adjust in response to the lower-hybrid drift instability according to the energy conservation law,

$$\begin{aligned} & W_i(0) + nT_e(0)/2 + nm_e v_{de}^2(0)/2 + \mathcal{E}(0) \\ &= W_i(t) + nT_e(t)/2 + nm_e v_{de}^2(t)/2 + \mathcal{E}(t) \end{aligned} \quad (5)$$

and the change of ion kinetic energy W_i (Fig. 1b) and the electric field energy $\mathcal{E}(t)$. Therefore, we model the implied changes in the electron kinetic energy and momentum by allowing the electron temperature T_e and drift velocity v_{de} to adjust in the linear electron susceptibility.

To incorporate the effect of anomalous transport in our simulations, the linear electron susceptibility is altered to accomodate v_{de} and T_e slowly changing in time. If time $n\Delta t \leq nth\Delta t$, both v_{de} and T_e are constant in time. Therefore, using a large value for nth allows us to simulate the linear regime of the instability without considering anomalous transport.

If time $t = n\Delta t > nth\Delta t$, we use the predictor-corrector scheme. Set predicted quantities v_{dep} and T_{ep} as

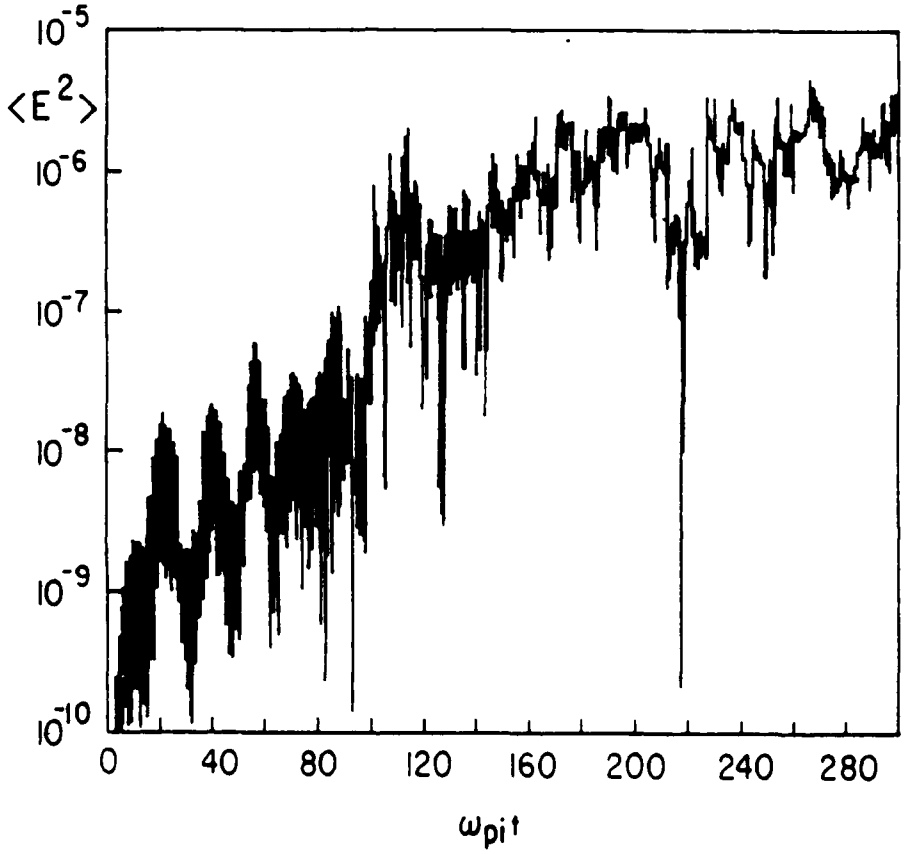

FIG. 2a. Electric field energy history plots for (a) time varying v_{de} and T_e (nth $\Delta t = 100$) and ...

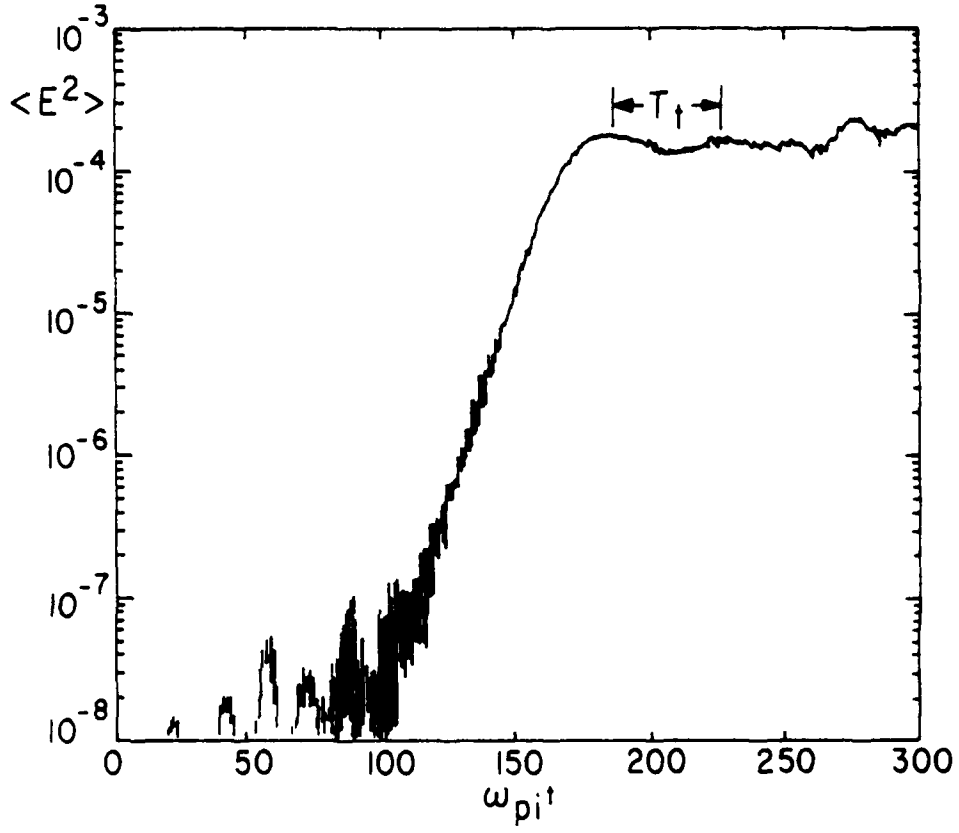

FIG. 2b. ... constant v_{de} and T_e. Parameters used are $m_i/m_e = 1600$, $\omega_{pe}^2/\omega_{ce}^2 = 1$, $T_e = 0$, $k\lambda_D = 1/\sqrt{2}$, $L_n/L_B = 0$, $L_n/L_T = 0$ and $v_E/v_{ti} = 0.57$.

$$v_{dep}^{n} = v_{de}^{n-1} \quad \text{and} \quad T_{ep}^{n} = T_{e}^{n-1} . \tag{6}$$

By solving Eq. (2), we get the predicted electric field E_p^n and field energy. Push the particle velocities from $v^{n-\frac{1}{2}}$ to $v_p^{n+\frac{1}{2}}$ by using E_p^n and calculate the predicted total ion kinetic energy W_{ip}^n and ion momentum P_{ip}^n by

$$W_{ip}^{n} = m_i \sum_{j=1}^{N} v_j^{n-\frac{1}{2}} v_{jp}^{n+\frac{1}{2}} \tag{7}$$

and

$$P_{ip}^{n} = \left(P_i^{n-\frac{1}{2}} + P_{ip}^{n+\frac{1}{2}} \right) /2 \tag{8}$$

where $P_{ip}^{n+\frac{1}{2}} = m_i \sum_{j=1}^{N} v_{jp}^{n+\frac{1}{2}}$. Now we use the corrector portion of the algorithm. Eq. (4) yields

$$v_{de}^{n} = v_{de}^{o} + (P_{ip}^{n} - P_i^{o})/nm_e \tag{9}$$

We substitute v_{de}^n into Eq. (5) and obtain

$$\frac{nT_e^n}{2} = \frac{nT_e^o}{2} + W_i^o + \mathcal{E}^o + \frac{nm_e v_{de}^{o\,2}}{2} - W_{ip}^n - \mathcal{E}_p^n - \frac{nm_e v_{de}^{n\,2}}{2} . \tag{10}$$

Substituting v_{de}^n and T_e^n into Eq. (2), we can solve the electric field E^n and the field energy $\mathcal{E}^n$.

Comparison of simulation results for time varying v_{de} and T_e with that for constant v_{de} and T_e is given in Figs. 2 and 3. Parameters used are $m_i/m_e = 1600.$, $\omega_{pe}^2/\omega_{ce}^2 = 1.$, $T_e = 0.$, $v_{ti} = (T_i/m_i)^{\frac{1}{2}} = 0.141421$, and $k\lambda_D = 0.707$. Fig. 2 for $v_E = 0.12$ and $nth\Delta t = 100$ shows that current relax-

ation stabilizes the lower-hybrid drift instability (Fig. 2a); otherwise ion trapping stabilizes the instability (Fig. 2b and Ref. 1). By assuming that the system stabilizes via current relaxation , the saturation level of the fluctuation spectrum was estimated at

$$\mathcal{E}_s = \frac{1}{2} \frac{N m_e v_{de}^2/2}{2(1+\omega_{pe}^2/\omega_{ce}^2)} \tag{12}$$

by Davidson (Ref. 2), and Davidson and Gladd (Ref. 3). The corresponding change in the ion temperature after saturation was given as

$$\frac{\Delta T_i}{T_i} \simeq 2\left(1 + \frac{\omega_{pe}^2}{\omega_{ce}^2}\right)\frac{\mathcal{E}_s}{NT_i} \tag{13}$$

for $T_e/T_i \ll 1$ and $v_E/v_{ti} \ll 1$. Similarly, we obtain

$$\frac{\Delta T_e}{T_i} \sim \frac{\omega_{pe}^2}{\omega_{ce}^2}\frac{\mathcal{E}_s}{NT_i} \tag{14}$$

as consequence of Eqs. (12), (13), momentum and energy conservation, Eqs. (4) and (5), and relaxing the relative drift v_d to zero. For the parameters we used, $\Delta T_e/T_i$ and $\Delta T_i/T_i$ are about 10^{-5}. The simulated saturation levels for both constant and time varying v_{de} and T_e compared with theories (Refs. 1, 2 and 3) are given in Fig. 3, indicating fairly good agreement. For cases in which $v_E < v_{ti}$ and v_d is allowed to relax in time, the saturation level of $\mathcal{E}_s/nT_i$ is so small that it is masked by the thermal flucatuations, whose level is equal to $\sim 10^{-5}$ in our simulations. Thus, no data appears on the curve labeled (b) in Fig. 3 for $v_E/v_{ti} < 0.8$.

FIG. 3. Comparison of saturation field energies as functions of v_E/v_{ti}. (a) For constant v_{de} and T_e, the lower-hybrid drift instability is saturated by ion trapping [1]. (b) For time varying v_{de} and T_e, saturation of the instability is achieved via current relaxation. The simulation data (dots in (a) and crosses in (b)) are in agreement with the theory shown by lines.

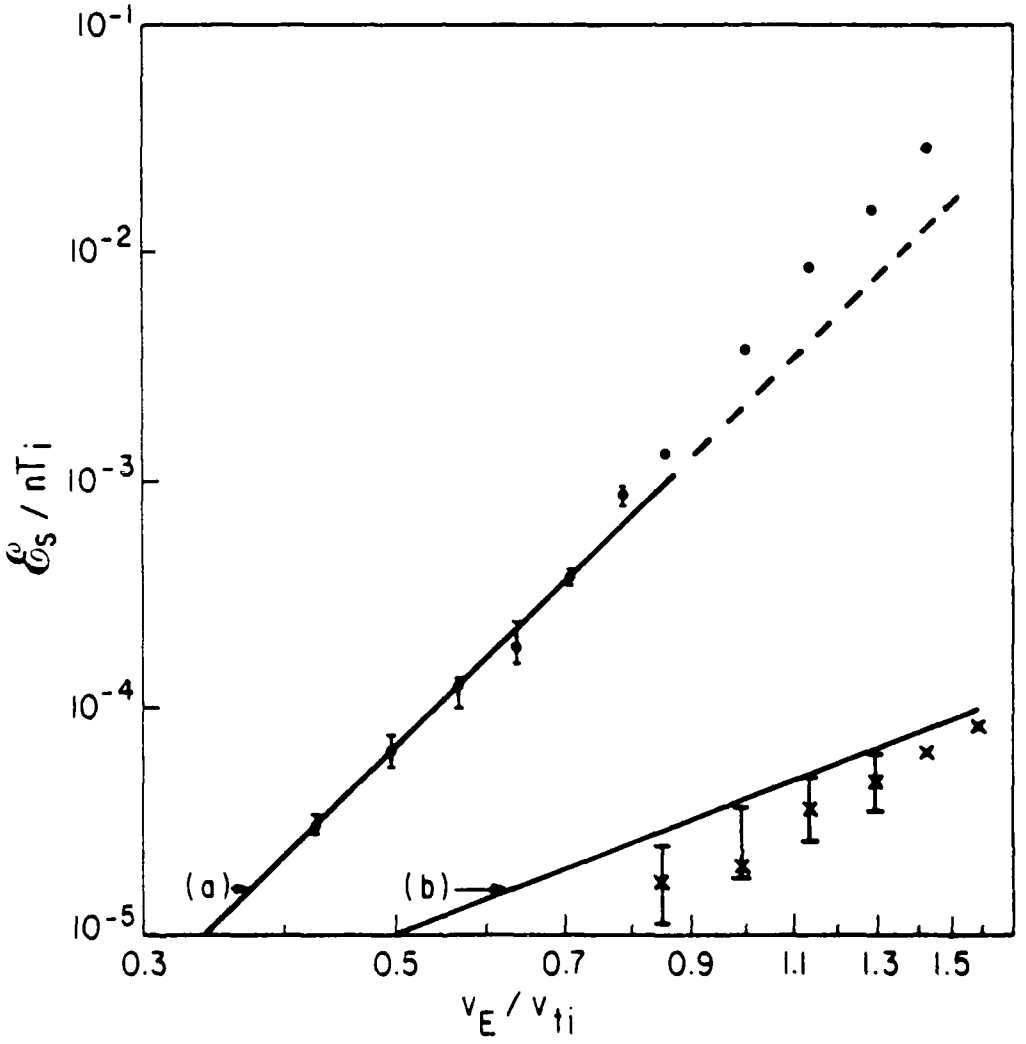

We would like to thank Dr. W. Nevins for several helpful discussions.

REFERENCES

1. Yu-Jiuan Chen, B. I. Cohen and C. K. Birdsall, "Lower-Hybrid Drift Instability Simulations Using ES1 Hybrid Code", QPR July-Sept. (1979).

2. R. C. Davidson, "Quasilinear Stabilzation of Lower-Hybrid Drift Instability", Phys. Fluids 21, 1375 (1978).

3. R. C. Davidson and N. T. Gladd, "Anomalous Transport Properties Associated with the Lower-Hybrid Drift Instability", Phys. Fluids 10, 1327 (1975).

B. CONTROL OF UNWANTED BEAMING INSTABILITY

(Prof. C. K. Birdsall)

Next quarter it is planned to look into instabilities which occur in magnetized plasmas with a Maxwellian or other $f(\underline{v})$ made up of rings in $v_\perp$ space at $t = 0$. The ring may be real (multivelocity neutral injection) or the result of loading for simulation. The multi-ring dispersion relation will be solved for complex ω and real k. Instabilities are expected even with a Maxwellian envelope. Simulations may be done to find saturation levels and detailed ring-ring interaction in order to aid in finding means to control these physical (but usually unwanted) instabilities.

C. FIELD REVERSED PLASMA SIMULATIONS, QUASINEUTRAL, IN 2d

Douglas Harned (Prof. C. K. Birdsall, Alex Friedman)

Progress has been made toward solving several problems that have arisen in our two-dimensional quasineutral code AQUARIUS. Much of the progress has consisted of debugging and adding improved diagnostics. Some of the difficulties originally encountered (e.g., noise, growing $\underline{E},\underline{J}$) in setting up cylindrical problems in cartesian coordinates have been reduced by

making the initialization more self-consistent. We are currently working on boundary conditions for a conducting wall boundary which are consistent with the quasineutral equations.

D. DISTRIBUTION FUNCTION AND CHARGE AND CURRENT DENSITIES IN LINEARIZED SIMULATIONS WITH CYLINDRICAL COORDINATES

Alex Friedman

In the following we derive appropriate expressions for the zero- and first-order distribution function associated with the k^{th} simulation superparticle. From these expressions we calculate charge and current densities. We then compare these results with the work of Bobroff[1], and make application to the RINGHYBRID 3d code[2]; axial displacements and current densities are omitted here as they are straightforward. The development presented here may be contrasted with that of Cohen et al., elsewhere in this QPR.

The distribution function $f_k(r,\theta,v_r,v_\theta)$ can be written

$$f_k = \frac{1}{2\pi}\int_0^{2\pi} d\phi\ S[r-r_k(\phi)]\ \frac{\delta[\theta-\theta_k(\phi)]}{r}\ \delta[\underline{v}-\underline{v}_k(r-\varepsilon_r e^{i\ell\phi},\phi)], \quad (1)$$

where ϕ parameterizes the unperturbed angular location of the element of the ring between ϕ and $\phi+d\phi$; ϕ and θ are both defined relative to the laboratory x-axis, and $\theta_k(\phi)$ is the angular location (in θ) of the point whose unperturbed location is ϕ. S is the finite-size-particle analogue of the δ-function. The particle velocity, $\underline{v}_k$, is a vector field since it differs for different points within the superparticle. In particular, to ensure a rigidly rotating zero-order superparticle (no shear to the motion), we must have

$$v^o_{\theta k}(r) = v^o_{\theta k}(r^o_k)\,\frac{r}{r^o_k} \equiv r\dot{\theta}\ , \tag{2}$$

where r^o_k is the radius of the "center" of the superparticle. Note that the flow velocity as a point in space (r,θ) arises from the motion of an element whose unperturbed location is $(r-\varepsilon_{rk}e^{i\ell\phi}\ ,\ \theta-\varepsilon_{\theta k}e^{i\ell\phi}/r)$, where $\varepsilon_k e^{i\ell\phi}$ is the perturbation from circularity. For rigid rotation $\varepsilon_{\theta k} = \varepsilon_{\theta k}(r^o_k)(r/r^o_k)$, and we have the relation:

$$\theta_k(\phi) = \phi + \frac{\varepsilon_{\theta k}(r^o_k)}{r^o_k}\ e^{i\ell\phi}\ . \tag{3}$$

Other expansions needed are:

$$\begin{aligned} r_k(\phi) &= r^o_k + \varepsilon_{rk}e^{i\ell\phi} \\ v_{rk}(\phi) &= v^o_{rk} + v^1_{rk}(\phi) \\ v_{\theta k}(r,\phi) &= v^o_{\theta k}(r^o_k)\,\frac{r}{r^o_k} + v^1_{\theta k}(r^o_k,\phi)\,\frac{r}{r^o_k} \end{aligned} \tag{4}$$

where

$$\begin{aligned} v^1_{rk}(\phi) &= (\dot{\varepsilon}_{rk} - \varepsilon_{\theta k}\dot{\theta})e^{i\ell\phi} \\ v^1_{\partial k}(\phi) &= (\dot{\varepsilon}_{\partial k} + \varepsilon_{rk}\dot{\theta})e^{i\ell\phi}\ . \end{aligned} \tag{5}$$

(The arguments (r), (r^o_k) have been omitted in the above for the sake of simplifying the notation; in the final expressions their locations will be evident.)

The zero-order distribution function is:

$$f_k^o = \frac{1}{2\pi r} S(r-r_k^o)\ \delta[\underline{v}-\underline{v}_k^o(r,\theta)] \ . \tag{6}$$

Integration over velocities yields the zero-order density:

$$n_k^o = \frac{1}{2\pi r} S(r-r_k^o) \ , \tag{7}$$

which satisfies the normalization condition $\int dr\ 2\pi r\ n_k^o(r) = 1$ if $\int dr\ S(r-r_k^o) = 1$, as for a δ-function (the limits of integration are 0 and r_{max}, the radius of the outer system boundary). For simplicity, so that we may freely interchange $\partial S/\partial r_k^o$ and $-\partial S/\partial r$, we demand $S(r-r_k^o)$ be a symmetric function of $(r-r_k^o)$. The zero-order azimuthal current density is:

$$\begin{aligned} J_{\theta k}^o &= \frac{1}{2\pi r} S(r-r_k^o) \int d^3v\ v_\theta\ \delta[\underline{v}-\underline{v}_k^o] \\ &= n_k^o(r)\ v_{\theta k}^o(r) = v_{\theta k}^o(r_k^o)\ S(r-r_k^o)/2\pi r_k^o \ , \end{aligned} \tag{8}$$

so that the algorithm used to accumulate $j_{\theta k}^o$ on a grid <u>differs</u> from that used for n_k^o if there is no shear; for the former one divides by the <u>particle</u> radius r_k^o, while for the latter division is by the <u>cell</u> radius r. Most codes with which the author is familiar use the same algorithm for weighting n_k^o and $j_{\theta k}^o$, and thus imply shear within the motion of each superparticle; this may have particular significance in gridded ("spokes and wheels") r-θ simulations where shear implies deformation of the particle, which is not permitted by the θ-weighting algorithm.

The first-order distribution function may be written as

$$f_k^1 = \frac{1}{2\pi r}\int_0^{2\pi} d\phi\ S[r-r_k^o-\varepsilon_{rk}e^{i\ell\phi}]\ \delta[\theta-\phi-\varepsilon_{\theta k}e^{i\ell\phi}/r_k^o]$$

$$\cdot\,\delta[\underline{v}-\underline{v}_k(r-\varepsilon_{rk}e^{i\ell\phi}\,,\,\theta-\varepsilon_{\theta k}e^{i\ell\phi}/r_k^o)] - f_k^o\,. \qquad (9)$$

Integration over velocities yields the first-order density:

$$n^1 = \frac{1}{2\pi r}\left\{-\varepsilon_r\frac{\partial}{\partial r}S(r-r^o)e^{i\ell\theta}\right.$$

$$\left.+\left[\int_0^{2\pi} d\phi\ \delta(\theta-\phi-\varepsilon_\theta e^{i\ell\phi}/r^o) - 1\right]S(r-r^o)\right\}\,, \qquad (10)$$

where subscripts k have been omitted for simplicity. Expansion of the term in square brackets yields $\int d\phi\ (\varepsilon_\theta/r^o)e^{i\ell\phi}\ \partial\delta(\theta-\phi)/\partial\phi$, and integration by parts yields $-i\ell\varepsilon_\theta e^{i\ell\theta}/r^o$. Use of Eq. (7) yields:

$$n^1 = \left[-\frac{\varepsilon_r}{r}\frac{\partial}{\partial r}r - \frac{i\ell\varepsilon_\theta}{r^o}\right]n^o e^{i\ell\theta}\,, \qquad (11)$$

which corresponds to Bobroff's expression [17] $\rho_1^{\text{Eulerian}}(\underline{r}_o,t) = -\nabla\cdot(\rho_o\underline{r}_1)$, where $\underline{r}_1$ is our $\underline{\varepsilon}e^{i\ell\theta}$ and ρ our n. With this information the first-order distribution function can be simplified. We have

$$\underline{v}_k(r-\varepsilon_r e^{i\ell\phi}\,,\,\theta-\varepsilon_\theta e^{i\ell\phi}/r^o)$$

$$= \underline{v}_k^o(r,\theta) - \frac{\varepsilon_\theta e^{i\ell\phi}}{r^o}\frac{\partial}{\partial\theta}\underline{v}_k^o(r,\theta) - \varepsilon_r e^{i\ell\phi}\frac{\partial}{\partial r}\underline{v}_k(r,\theta) + \underline{v}_k^1(r,\theta)\,, \qquad (12)$$

and using the relations $\partial\hat{r}/\partial\theta = \hat{\theta}$, $\partial\hat{\theta}/\partial\theta = -\hat{r}$ (carets denote unit vectors),

$$\underline{v}_k = \underline{v}_k^o(r,\theta) - \frac{\varepsilon_\theta e^{i\ell\phi}}{r^o}\,[v_r^o\hat{\theta}(\theta) - v_\theta^o(r)\hat{r}(\theta)]$$

$$- \varepsilon_r e^{i\ell\phi}\hat{\theta}\hat{\theta} + \underline{v}_k^1(r,\theta) \qquad (13)$$

$$= \underline{v}_k^o(r,\theta) - (\underline{\varepsilon}e^{i\ell\phi}\cdot\nabla)\underline{v}_k^o(r,\theta) + \underline{v}_k^1(r,\theta)\ ,$$

so that

$$\delta[\underline{v} - \underline{v}_k] - \delta[\underline{v} - \underline{v}_k^o]$$

$$= [(\underline{\varepsilon}e^{i\ell\phi}\cdot\nabla)\underline{v}_k^o - \underline{v}_k^1]\cdot\frac{\partial}{\partial\underline{v}}\,\delta[\underline{v} - \underline{v}_k^o]\ , \qquad (14)$$

and we obtain:

$$f^1 = n^1\delta[\underline{v}-\underline{v}^o(r,\theta)] + n^o[(\underline{\varepsilon}e^{i\ell\theta}\cdot\nabla)\underline{v}^o(r,\theta) - \underline{v}^1(r,\theta)]\cdot\frac{\partial}{\partial\underline{v}}\,\delta[\underline{v}-\underline{v}^o(r,\theta)]\ . \qquad (15)$$

Note that Eq. (13) might have been written down from first principles.

From this the first-order current may be calculated:

$$\underline{j}^1 = \int d^3v\ \underline{v}\ f^1$$

$$= n^1\underline{v}^o(r,\theta) + n^o\int d^3v\ \underline{v}\ [(\underline{\varepsilon}e^{i\ell\theta}\cdot\nabla)\underline{v}^o - \underline{v}^1]\cdot\frac{\partial}{\partial\underline{v}}\,\delta[\underline{v}-\underline{v}^o]\ , \qquad (16)$$

and integration by parts yields:

$$\underline{j}^1 = n^1\underline{v}^o(r,\theta) + n^o[\underline{v}^1(r,\theta) - (\underline{\varepsilon}e^{i\ell\phi}\cdot\nabla)\underline{v}^o(r,\theta)]\ . \qquad (17)$$

This expression is in agreement with Bogroff's Eq. [B63],

$$\underline{j}_1 = \rho^o\,[\frac{\partial}{\partial t}\,\underline{r}_1 + (\underline{v}_o\cdot\nabla)\underline{r}_1 - (\underline{r}_1\cdot\nabla)\underline{v}_o\,] - \underline{v}_o\nabla\cdot(\rho_o\underline{r}_1)\ ,\ [B63]$$

if we identify $\partial \underline{r}_1/\partial t + (\underline{v}_o \cdot \nabla)\underline{r}_1 = \underline{v}_1$ using Bobroff's [10] and our (11). Note that, explicitly,

$$\frac{\partial \underline{\varepsilon} e^{i\ell\theta}}{\partial t} = [-v_r^o(\varepsilon_\theta/r^o)\hat{\theta} + (\dot{\varepsilon}_r - i\ell\dot{\theta}\varepsilon_r)\hat{r} + (\dot{\varepsilon}_\theta - i\ell\dot{\theta}\varepsilon_\theta)\hat{\theta}]e^{i\ell\theta} \tag{18}$$

$$(\underline{v}_o \cdot \nabla)\underline{\varepsilon} e^{i\ell\theta} = [(i\ell\dot{\theta}\varepsilon_r - \dot{\theta}\varepsilon_\theta)\hat{r} + (i\ell\dot{\theta}\varepsilon_\theta + \dot{\theta}\varepsilon_r + v_r^o\varepsilon_\theta/r^o)\hat{\theta}]e^{i\ell\theta} \tag{19}$$

$$(-\underline{\varepsilon} e^{i\ell\theta} \cdot \nabla)\underline{v}^o = [\varepsilon_\theta \dot{\theta}\hat{r} - \varepsilon_\theta v_r^o/r^o\hat{\theta} - \varepsilon_r\dot{\theta}\hat{\theta}]e^{i\ell\theta} \ . \tag{20}$$

We may express the first-order current in component form by:

$$j_r^1 = \frac{1}{2\pi r}\left\{\left(\dot{\varepsilon}_r - i\ell\varepsilon_\theta\frac{v_r^o}{r^o}\right)S(r-r^o) - \varepsilon_r v_r{}^o\frac{\partial}{\partial r}S(r-r^o)\right\}e^{i\ell\theta}$$

$$j_\theta^1 = \frac{1}{2\pi r^o}\left\{\left(\dot{\varepsilon}_\theta - \varepsilon_\theta\frac{v_r^o}{r^o} - i\ell\dot{\theta}\varepsilon_\theta\right)S(r-r^o) - \varepsilon_r v_\theta^o\frac{\partial}{\partial r}S(r-r^o)\right\}e^{i\ell\theta} \ . \tag{21}$$

Note the presence of r and r^o in the demominators of j_r^1, j_θ^1, respectively.

(An alternative derivation of $\underline{J}^1$ uses the identity:

$$\int_0^{2\pi} d\phi\left\{\frac{\varepsilon_\theta e^{i\ell\phi}}{r^o}\frac{\partial}{\partial\phi}\delta[\theta-\phi]\right\}\delta[\underline{v}-\underline{v}^o]$$

$$= -\int_0^{2\pi} d\phi\ \delta[\theta-\phi]\frac{\partial}{\partial\phi}\left\{\frac{\varepsilon_\theta e^{i\ell\phi}}{r^o}\delta[\underline{v}-\underline{v}^o]\right\}$$

$$= -\frac{i\ell\varepsilon_\theta}{r^o}e^{i\ell\theta}\delta[\underline{v}-\underline{v}^o] - \frac{\varepsilon_\theta e^{i\ell\theta}}{r^o}\frac{\partial}{\partial\theta}\delta[\underline{v}-\underline{v}^o(\theta)] \ . \tag{22}$$

The first term gives part of $n^1 v^o$; the second gives part of $(-\underline{\varepsilon} e^{i\ell\theta}\cdot\nabla)\underline{v}^o$, since

$$\frac{\partial}{\partial\theta}\,\delta[\underline{v}-\underline{v}^o] \;=\; [-v_r^o\hat{\theta} + v_\theta^o\hat{r}]\cdot\frac{\partial}{\partial\underline{v}}\,\delta[\underline{v}-\underline{v}^o] \qquad (23)$$

through use of the "Chain Rule" of calculus.

Using the results of Bobroff it is not difficult to show that charge continuity, $\nabla\cdot\underline{j}^1 + \partial\rho^1/\partial t = 0$, is safisfied. An alternative expression for the first-order current is Bobroff's [B57]:

$$\underline{j}^1 \;=\; \partial(\rho_o\underline{r}^1)/\partial t + \nabla\times(\rho_o\underline{r}^1\times\underline{v}^o)\ . \qquad [B57]$$

Taking the divergence of this expression gives $\nabla\cdot\underline{j}^1 = \partial(\nabla\cdot\rho_o\underline{r}^1)/\partial t$ which is $-\partial\rho^1/\partial t$ by (11).

As a check on the calculation, the continuity equation can be vefified directly from our final expressions for n^1, $\underline{j}^1$. Since $\underline{\varepsilon}$ is defined as a moving point which at the old time level is at angle $\alpha = 0$ and at the new time level is at $\alpha = \dot{\theta}\Delta t$, we must rotate n^{1new} back to the x-axis through an angle $\ell\dot{\theta}\Delta t$:

$$-\frac{\partial n^1}{\partial t} \;=\; \frac{1}{2\pi r}\frac{\partial}{\partial r}\left[\varepsilon_r^{new}\,S(r-r^{new})\,e^{-i\ell\dot{\theta}\Delta t} - \varepsilon_r^{old}\,S(r-r^{old})\right]/\Delta t$$

$$+\ \frac{i\ell}{2\pi r}\left[\frac{\varepsilon_\theta^{new}}{r^{new}}\,S(r-r^{new})\,e^{-i\ell\dot{\theta}\Delta t} - \frac{\varepsilon_\theta^{old}}{r^{old}}\,S(r-r^{old})\right]/\Delta t$$

$$=\ \frac{1}{2\pi r}\frac{\partial}{\partial r}\Big[\underset{\{1\}}{(\dot{\varepsilon}_r}\ \underset{\{4\}}{-i\ell\dot{\theta}\varepsilon_r)S}\ -\ \underset{\{2\}}{\varepsilon_r v_r^o}\,\partial S/\partial r\Big]$$

$$+\ \frac{i\ell}{2\pi r}\left[\underset{\{5\}}{\left(\frac{\dot{\varepsilon}_\theta}{r^o}\right.}\ -\ \underset{\{6\}}{\left.\frac{i\ell\dot{\theta}\varepsilon_\theta}{r^o}\right)S}\ -\ \underset{\{3a\}}{\frac{\varepsilon_\theta v_r^o}{r^o}\frac{\partial S}{\partial r}}\ -\ \underset{\{3b\}}{\frac{\varepsilon_\theta v_r^o}{r^{o2}}S}\right]. \qquad (24)$$

Taking the divergence of expressions (21) yields:

$$\nabla\cdot\underline{j}^1 = \frac{1}{2\pi r}\frac{\partial}{\partial r}\left[(\dot{\varepsilon}_r - i\ell\varepsilon_\theta v_r^o/r^o)S - \varepsilon_r v_r^o \partial S/\partial r \right] \qquad (25)$$

$$\{1\} \quad \{3a\} \quad \{2\}$$

$$+ \frac{i\ell}{2\pi r r^o}\left[(\dot{\varepsilon}_\theta - \varepsilon_\theta v_r^o/r^o - i\ell\dot{\theta}\varepsilon_\theta)S - \varepsilon_r v_\theta^o \partial S/\partial r \right] \qquad (25)$$

$$\{5\} \quad \{3b\} \quad \{6\} \quad \{4\}$$

so that the two expressions are in agreement. An alternate derivation of $\partial n^1/\partial t$ involves writing it as $-\nabla\cdot(\partial n^o/\partial t)\underline{r}^1 - \nabla\cdot n^o \partial \underline{r}^1/\partial t$ and recognizing that $\partial n^o/\partial t = (-v_r^o/2\pi r)\partial S/\partial r$.

Another alternate derivation uses the relation

$$\frac{\partial n^1}{\partial t} = \frac{dn^1}{dt} - \underline{v}^o\cdot\nabla n^1$$

$$= \left[\frac{\dot{\varepsilon}_r}{2\pi r}\frac{\partial S}{\partial r} + \frac{i\ell\dot{\varepsilon}_\theta}{2\pi r r^o}S - \frac{i\ell\varepsilon_\theta v_r^o}{2\pi r r^{o2}}S\right] - \frac{v_r^o}{r}\left[\frac{\varepsilon_r}{2\pi r}\frac{\partial S}{\partial r} + \frac{i\ell\varepsilon_\theta}{2\pi r r^o}S\right]$$

$$\{1\} \quad \{5\} \quad \{3\} \qquad \{2\} \quad \{3\}$$

$$- v_r^o\frac{\partial}{\partial r}\left[\frac{\varepsilon_r}{2\pi r}\frac{\partial S}{\partial r} + \frac{i\ell\varepsilon_\theta}{2\pi r r^o}S\right] - i\ell\dot{\theta}\left[\frac{\varepsilon_r}{2\pi r}\frac{\partial S}{\partial r} + \frac{i\ell\varepsilon_\theta}{2\pi r r^o}S\right].$$

$$\{2\} \quad \{3\} \qquad \{4\} \quad \{6\}$$

The $v_r^o\partial/\partial r$ and v_r^o/r terms combine to yield a $(v_r^o/r)(\partial/\partial r)r$ term, and there are factors of $1/2\pi r$ in n^1. Also, n^1 decreases (even at the center of the ring) as the ring moves outward ($v_r^o > 0$) because of the division by the increasing value of r(ring center), hence the v_r^o/r term in dn^1/dt.

********** ********** ********** **********

As an example, we consider the displacement off-axis ($\ell = 1$) of an infinite current layer in a uniform field. The equations of motion are:

$$\ddot{\varepsilon}_r - \varepsilon_r\dot{\theta}^2 - 2\dot{\varepsilon}_\theta\dot{\theta} = -\dot{\theta}(\dot{\varepsilon}_\theta + \varepsilon_r\dot{\theta})$$

$$\ddot{\varepsilon}_\theta - \varepsilon_\theta\dot{\theta}^2 + 2\dot{\varepsilon}_r\dot{\theta} = \dot{\theta}(\dot{\varepsilon}_r - \dot{\varepsilon}_\theta\dot{\theta})$$

or

$$\dot{\varepsilon}_r = \dot{\theta}\varepsilon_\theta \quad , \quad \dot{\varepsilon}_\theta = -\dot{\theta}\varepsilon_r \, .$$

Furthermore, if the vectorial first order displacement of a point is to remain constant as the point gyrates, we must have $\dot{\varepsilon}_r = i\dot{\theta}\varepsilon_r$, $\dot{\varepsilon}_\theta = i\dot{\theta}\varepsilon_\theta$. Compatibility of these with the above requires

$$\varepsilon_\theta = i\varepsilon_r \quad , \quad \dot{\varepsilon}_r = i\dot{\theta}\varepsilon_r \quad , \quad d/dt = i\dot{\theta}$$

where d/dt is the rate of change of a quantity (such as ε_r) along a particle orbit.

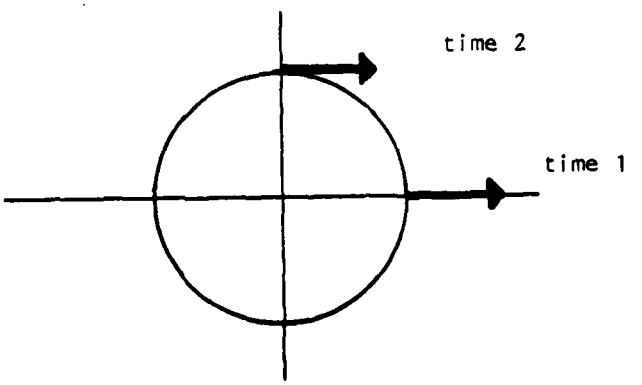

If motion $\propto e^{-i\omega t}$ is assumed, $\omega = -\dot{\theta}$, indicating that the comoving coordinate axes rotate in the $+\theta$ direction, so components of a constant vector in comoving coordinates rotate in the $-\theta$ direction.

REFERENCES

1. D. L. Bobroff, IRE Trans. PGED ED-6, 68 (1959).

2. A. Friedman, R. N. Sudan, and J. Denavit, "A Linearized 3-D Hybrid Code for Stability Studies of Field-Reversed Ion Rings", Cornell Univ. LPS Rept. No. 268 (1979), submitted to J. Comp. Phys.

[NOTE: *The following was contributed by colleagues at LLL, a result of considerable mutual discussion.*]

E. SOME CONSERVATION PROPERTIES OF LINEARIZED PARTICLE CODES

B. I. Cohen, S. P. Auerbach, and J. A. Byers
Lawrence Livermore Laboratory, University of California
Livermore, California 94550

and H. Weitzner
Courant Institute of Mathematical Sciences, New York University,
New York, New York 10003

ABSTRACT

Conservation laws are derived which are appropriate for use in linearized particle simulation codes. A continuity equation describing mass or charge conservation and an extended Poynting theorem describing energy flow are obtained for general curvilinear coordinate systems. These conservation equations are expressed in terms of quantities readily calculable in a particle code, serve to quantitatively assess the validity and precision of code results, and provide valuable insight into the physics being studied. A conserved quantity related to the system energy, rather than a Poynting theorem, is derived from a Lagrangian formulation. It is bilinear in first order quantities but is not attractive for implementation as a diagnostic in a linearized particle simulation.

I. INTRODUCTION

Particle simulation provides a powerful tool for assessing the stability of complex plasma equilibria, wherein kinetic effects play an essential role. Of special interest is the recent use of linearized particle codes[1-5] to study the stability of equilibria for which analytical methods are not available. These codes solve the linearized equations of motion for small deviations of the particle orbits and electromagnetic fields from their equilibrium values. Compared to fully nonlinear simulations, linearized simulations possess certain advantages. By means of linearization and Fourier analysis the computer economics of two- and three-dimensional simulation are greatly improved.[4,5] Furthermore, highly accurate determination of linear growth rates is possible; this is often very difficult in fully nonlinear simulations because of high thermal fluctuation levels and relatively short growth periods terminated by nonlinear saturation.

Linearized codes are particularly relevant to situations in which the dimensionless ratio of a characteristic parameter associated with particle dynamics to a characteristic parameter associated with either the equilibrium configuration or a coherent oscillation of the plasma is of order unity, so that an analytical perturbation expansion is not possible. Examples of importance in the study of fusion plasmas occur when the characteristic dimension of a particle trajectory, for example, the electron or ion Larmor radius in a magnetized plasma, is comparable to either the length over which the plasma equilibrium varies or the wavelength of an unstable mode.

In this article we investigate certain conservation properties of linearized particle codes. Conservation laws are valuable in at least two different ways: they provide quantitative means of monitoring the accuracy and validity of a simulation and can furnish considerable insight into the details of, for example, particle and energy transport accompanying the linear phase of an instability. These conservation laws act as the basis for code diagnostics that only require simple computations involving readily available simulation quantities. Particular attention will be given to the form these expressions take when curvilinear coordinates are used.

It is not a trivial task to develop conservation laws for linearized particle or fluid models. This is because, by definition, in a linearized system there are only quantities that are linear in a perturbation and no terms of second or higher order. The difficulty this poses can be seen by considering as an example particle kinetic energy. With particle velocity given by $\vec{v} = \vec{v}_0 + \varepsilon\vec{v}_1 + \varepsilon^2 \vec{v}_2 + \ldots$, where ε is a small parameter measuring deviation from equilibrium, the kinetic energy is $K = (m/2) \times[v_0^2 + 2\varepsilon\vec{v}_0 \cdot \vec{v}_1 + \varepsilon^2 (v_1^2 + 2\, \vec{v}_0 \cdot \vec{v}_2) + \ldots]$. Typically, the first order terms (proportional to ε) will vanish when K is summed over particles. The second order kinetic energy, when summed over all particles, plus the analogous electric and magnetic field quantities will be conserved as a consequence of the particle equations of motion and Maxwell's equations. However, this conservation law is useless in a linearized code, which does not calculate $\vec{v}_2$ nor the deviations of the electromagnetic fields at second order. Thus, we have taken as our task the derivation of conserved quantities which are sums of terms bilinear in the first order quantities computed by linearized codes.

The contents of this article are organized as follows. Section 2 contains a derivation of the linearized perturbed charge and current densities for general coordinate systems. Specific conservation laws, e.g., continuity of charge (or mass) and a Poynting theorem describing energy flow, are derived in Section 3. We recover the results of earlier researchers[6,7] in the cold fluid limit (Sec. 4). Illustrations of the conservation laws are presented in Section 5.

II. PERTURBED CHARGE AND CURRENT DENSITIES

In this section we derive the linearized perturbed charge and current densities. We shall adopt a general Klimontovich representation that is independent of the particular choice of coordinate system.[8] For a collisionless plasma satisfying the Vlasov equation,

$$\frac{\partial f}{\partial t} + \vec{v} \cdot \frac{\partial f}{\partial \vec{x}} + \vec{a} \cdot \frac{\partial f}{\partial \vec{v}} = 0 \quad , \tag{1}$$

where $f = f(\vec{x},\vec{v};t)$ is the usual phase-space distribution function, the distribution function is formally given by

$$f(\vec{x},\vec{v},t) = \left\langle \sum_i \delta(\vec{x}_i - \vec{x})\ \delta(\vec{v}_i - \vec{v}) \right\rangle \quad , \tag{2}$$

where the summation is over particles and $\vec{x}_i(t)$, $\vec{v}_i(t)$ satisfy

$$\frac{d}{dt}\vec{x}_i = \vec{v}_i \tag{3a}$$

$$\frac{d}{dt}\vec{v}_i = \vec{a}(\vec{x} = \vec{x}_i;t) \quad . \tag{3b}$$

The brackets in Eq. (2) indicate that an average over particle initial conditions has been performed, which is equivalent to a coarse-grained average of the many-particle distribution function. In a simulation plasma, particles are finite in size; and the shape function $S(\vec{x}_i - \vec{x})$ replaces the delta function $\delta(\vec{x}_i - \vec{x})$.[9] Interpolation of charge and current densities onto a spatial grid from a large number of particles per cell and solution of Maxwell's equations on the grid for the macroscopic fields accomplish the necessary coarse-grained average in the simulation.[9] Henceforth in our analysis we drop the brackets in Eq. (2) and presume that the averaging is understood.

The unperturbed distribution function is constructed from the unperturbed trajectories,

$$f^{(0)}(\vec{x},\vec{v};t) = \sum_i \delta\left(\vec{x}_i^{(0)} - \vec{x}\right) \delta\left(\vec{v}_i^{(0)} - \vec{v}\right) \quad , \tag{4}$$

where $\vec{x}_i^{(0)}(t)$ and $\vec{v}_i^{(0)}(t)$ are the equilibrium position and velocity. The linearized perturbed distribution function is then given by

$$f^{(1)} = \sum_i \delta\left(\vec{x}_i^{(0)} + \vec{x}_i^{(1)} - \vec{x}\right) \delta\left(\vec{v}_i^{(0)} + \vec{v}_i^{(1)} - \vec{v}\right) - f^{(0)} \quad , \tag{5a}$$

which leads to

$$f^{(1)} = -\sum_i \vec{x}_i^{(1)} \cdot \frac{\partial}{\partial \vec{x}} \delta\left(\vec{x} - \vec{x}_i^{(0)}\right) \delta\left(\vec{v} - \vec{v}_i^{(0)}\right)$$

$$- \sum_i \vec{v}_i^{(1)} \cdot \frac{\partial}{\partial \vec{v}} \delta\left(\vec{v} - \vec{v}_i^{(0)}\right) \delta\left(\vec{x} - \vec{x}_i^{(0)}\right) \tag{5b}$$

upon expansion in a Taylor series. $\vec{x}_i^{(1)}$ and $\vec{v}_i^{(1)}$ are position and velocity displacements relative to the unperturbed trajectories (Fig. 1).

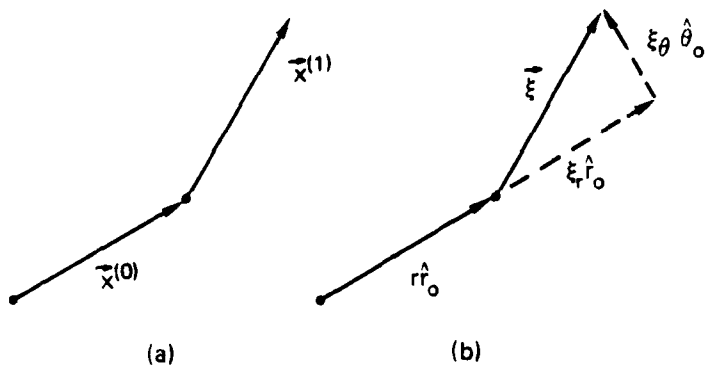

Figure 1. Particle displacement in a linearized code, (a) general representation and (b) representation in polar coordinates.

This brings in a Lagrangian aspect to the calculation and has been formally described as a polarization representation in the excellent treatment given by Bobroff.[6]

Calculation of the perturbed charge and current densities from Eq. (5b) is simple and direct. The linearized perturbed number density $n^{(1)}$ for each species is

$$n^{(1)} = \int d^3\vec{v}\, f^{(1)} = - \sum_i \vec{x}_i^{(1)} \cdot \frac{\partial}{\partial \vec{x}} \delta\left(\vec{x} - \vec{x}_i^{(0)}\right) \quad , \tag{6}$$

because the spatial and velocity-space divergences $(\partial/\partial\vec{x})\cdot$ and $(\partial/\partial\vec{v})\cdot$ of the particle displacements $\vec{x}_i^{(0)}$, $\vec{x}_i^{(1)}$ and velocities $\vec{v}_i^{(0)}$, $\vec{v}_i^{(1)}$ are identically zero. Similarly, the linearized current density $\vec{J}^{(1)}$ is given by

$$\vec{J}^{(1)} = e \int d^3v\, \vec{v} f^{(1)} = - e \sum_i \vec{v}_i^{(0)}\, \vec{x}_i^{(1)} \cdot \frac{\partial}{\partial \vec{x}} \delta\left(\vec{x} - \vec{x}_i^{(0)}\right) + e \sum_i \vec{v}_i^{(1)}\, \delta\left(\vec{x} - \vec{x}_i^{(0)}\right) \tag{7}$$

Alternate expressions for $n^{(1)}$ and $\vec{J}^{(1)}$ can be obtained with use of simple vector calculus identities,

$$n^{(1)} = - \frac{\partial}{\partial \vec{x}} \cdot \sum_i \vec{x}_i^{(1)}\, \delta\left(\vec{x} - \vec{x}_i^{(0)}\right) \tag{8}$$

and

$$\vec{J}^{(1)} = - e \frac{\partial}{\partial \vec{x}} \cdot \sum_i \vec{v}_i^{(0)}\, \vec{x}_i^{(1)}\, \delta\left(\vec{x} - \vec{x}_i^{(0)}\right) + e \sum_i \vec{v}_i^{(1)}\, \delta\left(\vec{x} - \vec{x}_i^{(0)}\right) . \tag{9}$$

We observe that in Eqs. (8) and (9) the derivatives $(\partial/\partial\vec{x})$ have been commuted with the summation over particles. This allows the derivative to

be calculated on the grid in the simulation code, and the derivative of the shape function does not then enter explicitly.

Use of the identities employed in deriving Eqs. (8) and (9) yields yet another expression for the linearized current density[6]

$$\vec{J}^{(1)} = e \frac{\partial}{\partial t} \sum_i \vec{x}_i^{(1)} \left(\vec{x} - \vec{x}_i^{(0)} \right) + \frac{\partial}{\partial \vec{x}} \times \sum_i \vec{x}_i^{(1)} \times \vec{v}_i^{(0)} \delta \left(\vec{x} - \vec{x}_i^{(0)} \right) . \qquad (10)$$

Equation (10) has the important computational advantage over Eq. (9) in that a curl of a vector is required rather than a divergence of a tensor. Appropriate care must be exercised in evaluating divergences, curls, and other spatial differential operators when curvilinear coordinates are used, which in our personal experience has been a frequent source of difficulty in both analysis and code development.

To evaluate Eqs. (6) and (7), or (8) and (9), the zero and first order particle trajectories need to be determined. This in turn requires the electric and magnetic fields, which typically are derived by solution of Maxwell's equations on an Eulerian mesh given sources $n^{(1)}$ and $\vec{J}^{(1)}$. The forces on and hence the acceleration of the particles are deduced from the electric and magnetic fields evaluated along the particle trajectories.

To illustrate the polarization representation and to prepare the groundwork for examples that are considered in Sec. 5, we consider cylindrical coordinates for a system that is axisymmetric at zero order (Fig. 1). The velocity vector is given by

$$\vec{v} = \vec{v}^{(0)} + \vec{v}^{(1)} = \frac{d}{dt} \vec{x}^{(0)} + \frac{d}{dt} \vec{x}^{(1)} = \frac{d}{dt} \left(r_0 \hat{r}_0 + z_0 \hat{z} + \xi_r \hat{r}_0 + \xi_\theta \hat{\theta}_0 + \xi_z \hat{z} \right)$$

$$= \dot{r}_0 \hat{r}_0 + r_0 \dot{\theta}_0 \hat{\theta}_0 + \dot{z}_0 \hat{z}_0 + (\dot{\xi}_r - \xi_0 \dot{\theta}_0) \hat{r}_0 + (\dot{\xi}_\theta + \xi_r \dot{\theta}_0) \hat{\theta}_0 + \dot{\xi}_z \hat{z}_0 \quad , \qquad (11)$$

where $d\hat{r}_0/dt = \dot{\theta}_0\hat{\theta}_0$, $d\hat{\theta}_0/dt = -\dot{\theta}_0\hat{r}_0$, $\dot{r}_0 \equiv dr_0/dt$, $\dot{\theta}_0 \equiv d\theta_0/dt$, etc. From Eq. (10) identification of the velocity components is obvious,

$$(v_r , v_\theta , v_z)^{(0)} = (\dot{r}_0, r_0\dot{\theta}_0, \dot{z}_0) \tag{12}$$

and

$$\left(v_r , v_\theta , v_z\right)^{(1)} = \left(\dot{\xi}_r - \xi_\theta \dot{\theta}_0, \dot{\xi}_\theta + \xi_r\dot{\theta}_0, \dot{\xi}_z\right) \quad . \tag{13}$$

III. CONSERVATION LAWS

A. Continuity

Integration of the Vlasov equation, Eq. (1), over velocity space yields the continuity equation

$$\frac{\partial n}{\partial t} + \frac{\partial}{\partial \vec{x}} \cdot \frac{\vec{J}}{e} = 0 \quad . \tag{14}$$

Continuity of charge (or mass) at lowest order is easily demonstrated with use of $n^{(0)} = \sum_i \delta(\vec{x} - \vec{x}_i^{(0)})$, and $\vec{J}^{(0)} = e\sum_i \vec{v}_i^{(0)}\ \delta(\vec{x} - \vec{x}_i^{(0)})$,

$$\partial n^{(0)}/\partial t = -\sum_i \left(\vec{dx}_i^{(0)}/dt\right) \cdot (\partial/\partial\vec{x})\ \delta\left(\vec{x} - \vec{x}_i^{(0)}\right)$$

$$= -(\partial/\partial\vec{x}) \cdot \sum_i \vec{v}_i^{(0)}\ \delta\left(\vec{x} - \vec{x}_i^{(0)}\right) = -(\partial/\partial\vec{x}) \cdot \vec{J}^{(0)}/e$$

At first order, differentiation of Eq. (8) with respect to time leads to

$$\frac{\partial n^{(1)}}{\partial t} = -\frac{\partial}{\partial \vec{x}} \cdot \sum_i \left[\vec{v}_i^{(0)}\ \delta\left(\vec{x} - \vec{x}_i^{(0)}\right) - \vec{x}_i^{(1)}\ \vec{v}_i^{(0)} \cdot \frac{\partial}{\partial \vec{x}}\delta\left(\vec{x} - \vec{x}_i^{(0)}\right)\right] \quad , \tag{15}$$

where $\vec{v}_i^{(1)} \equiv d\vec{x}_i^{(1)}/dt$ and $\vec{v}_i^{(0)} \equiv d\vec{x}_i^{(0)}/dt$. Because $(\partial/\partial\vec{x}) \cdot \vec{v}_i^{(0)} = (\partial/\partial\vec{x}) \cdot \vec{x}_i^{(1)} \equiv 0$, the second term on the right side of Eq. (15) can be rewritten as $-(\partial/\partial\vec{x}) \cdot \vec{v}_i^{(0)}\, \vec{x}_i^{(1)}\, \delta(\vec{x} - \vec{x}_i^{(0)})$. We then recognize that Eq. (15) is just the divergence of Eq. (9) multiplied by (-1), i.e.,

$$\frac{\partial n^{(1)}}{\partial t} + \frac{\partial}{\partial \vec{x}} \cdot \frac{\vec{J}^{(1)}}{e} = 0 \tag{16}$$

The same result is obtained even more directly by using Eq. (10).

B. Poynting Theorem

Similar conservation laws can be calculated by multiplying the Vlasov equation by increasing powers of $\vec{v}$ and deducing the corresponding moment equations. Of interest here is the energy flow in a linearized simulation. The linearized Maxwell equations are

$$\vec{\nabla} \times \vec{B}^{(1)} = \frac{4\pi\vec{J}^{(1)}}{c} + \frac{\partial\vec{E}^{(1)}}{c\partial t} \tag{17a}$$

$$\vec{\nabla} \times \vec{E}^{(1)} = -\frac{\partial\vec{B}^{(1)}}{c\partial t} \tag{17b}$$

$$\vec{\nabla} \cdot \vec{B}^{(1)} = 0 \tag{17c}$$

From the scalar products of Eq. (17a) with $\vec{E}^{(1)}$ and Eq. (17b) with $\vec{B}^{(1)}$, we obtain

$$\frac{\partial}{\partial t}\left(\frac{E^{(1)2}}{8\pi} + \frac{B^{(1)2}}{8\pi}\right) + \frac{c}{4\pi}\nabla \cdot \left(\vec{E}^{(1)} \times \vec{B}^{(1)}\right) = -\vec{E}^{(1)} \cdot \vec{J}^{(1)} \ . \tag{18}$$

This is a Poynting theorem that is bilinear in perturbed quantities. Because Maxwell's equations are "linear," the same manipulations lead to

Poynting theorems that are bilinear in field and current perturbations of arbitrary order. (In typical applications, the Poynting theorem constructed from zero order quantities may be especially simple, if not trivial, due to the symmetry and/or simplicity of the equilibrium, e.g., $\vec{B}^{(0)} = B_0\hat{Z}$, B_0 = constant, and $\vec{E}^{(0)} = \vec{J}^{(0)} = 0$.)

Monitoring the equality of the left and right sides of Eq. (18) in a linearized simulation would only check the accuracy of the numerical solution of Maxwell's equations and would give no information on the validity and self-consistency of the particle trajectories. To make further progress we must explicitly evaluate $\vec{E}^{(1)} \cdot \vec{J}^{(1)}$.

The linearized equation of motion is given by

$$\left(\frac{m}{e}\right) \frac{d\vec{v}^{(1)}}{dt} = \vec{E}^{(1)}_{tot} + \frac{\vec{v}^{(0)} \times \vec{B}^{(1)}_{tot}}{c} + \frac{\vec{v}^{(1)} \times \vec{B}^{(0)}}{c} \tag{19a}$$

where

$$\vec{E}^{(1)}_{tot} = \vec{E}^{(1)}\left(\vec{x}^{(0)}\right) + \vec{x}^{(1)} \cdot \frac{\partial}{\partial \vec{x}} \vec{E}^{(0)}\left(\vec{x}^{(0)}\right) \tag{19b}$$

$$\vec{B}^{(1)}_{tot} = \vec{B}^{(1)}\left(\vec{x}^{(0)}\right) + \vec{x}^{(1)} \cdot \frac{\partial}{\partial \vec{x}} \vec{B}^{(0)}\left(\vec{x}^{(0)}\right) \quad . \tag{19c}$$

The scalar product of Eq. (19a) with $\vec{v}^{(1)}$ gives

$$\frac{d}{dt} \frac{mv^{(1)^2}}{2} = e\,\vec{v}^{(1)} \cdot \vec{E}^{(1)} + e\,\vec{v}^{(1)} \cdot \left(\vec{x}^{(1)} \cdot \frac{\partial}{\partial \vec{x}}\right) \vec{E}^{(0)}$$

$$+ e\,\vec{v}^{(1)} \cdot \frac{\vec{v}^{(0)}}{c} \times \left(\vec{B}^{(1)} + \vec{x}^{(1)} \cdot \frac{\partial \vec{B}^{(0)}}{\partial \vec{x}}\right) \quad , \tag{20}$$

where all field quantities are evaluated at $\vec{x}^{(0)}$. Use of Eq. (9) for $J^{(1)}$ and integration by parts lead to

$$\int d^3x\, \vec{E}^{(1)} \cdot \vec{J}^{(1)} = e \sum_i \vec{v}^{(1)} \cdot \vec{E}^{(1)} + e \sum_i \vec{v}_i^{(0)} \cdot \left(\vec{x}_i \cdot \frac{\partial}{\partial \vec{x}} \right) \vec{E}^{(1)} \quad . \tag{21}$$

Integration of Eq. (18) over volume and substitution of Eqs. (20) and (21) yield

$$\frac{d}{dt}\left[\int d^3x \left(\frac{E^{(1)2}}{8\pi} + \frac{B^{(1)2}}{8\pi} \right) + \sum_i \frac{1}{2} m v_i^{(1)2} \right] + \frac{c}{4\pi} \int ds\, \hat{n} \cdot \left(\vec{E}^{(1)} \times \vec{B}^{(1)} \right) =$$

(22)

$$\sum_i \left[e\, \vec{v}_i^{(1)} \cdot \left(\vec{x}_i^{(1)} \cdot \frac{\partial}{\partial \vec{x}} \right) \vec{E}^{(0)} - e\, \vec{v}_i^{(0)} \cdot \left(\vec{x}_i \cdot \frac{\partial}{\partial \vec{x}} \right) \vec{E}^{(1)} + e\, \vec{v}_i^{(1)} \cdot \left(\frac{\vec{v}_i^{(0)}}{c} \times \vec{B}_{tot}^{(1)} \right) \right],$$

where all the field quantities within the summation over particles are evaluated at $\vec{x}_i^{(0)}$ and $\hat{n}$ is the unit normal to the surface containing the volume of integration. We have obtained the same result starting from the Low Lagrangian.[10]

We observe that Eq. (22) is an extended Poynting theorem and that its right side is not zero in general. In fact, the right side cannot vanish if the linearized system exhibits growth or damping and appropriate boundary conditions are adopted so that the Poynting flux $(c/4\pi)\, \vec{E}^{(1)} \times \vec{B}^{(1)}$ vanishes at the surface of the volume (e.g., periodic boundary conditions, a conducting boundary, or vanishing fields at infinity), because the remaining terms on the left side are positive-definite. The right side of Eq. (22) is bilinear in first order quantities and also contains zero order flow and field quantities. This allows free energy at zero order to be exchanged with first order quantities.

C. Energy Conservation

An energy conservation law, rather than a Poynting theorem, can in fact be derived. Oberman and Dawson[11] have shown that

$$\frac{d}{dt}\left[\int dx \left(\frac{E^{(1)2}}{8\pi} + \frac{B^{(1)2}}{8\pi}\right) + \sum_s \iint dx dv \frac{m v f_s^{(1)}}{2\partial f_s^{(0)}/\partial v}\right] = 0 \qquad (23)$$

in one dimension. Although Eq. (23) is often described as an energy conservation law, a similar equation can be derived from invoking conservation of entropy, as can be demonstrated by considering the expansion of the quantity $-f\ell nf$ to second order in small perturbations from thermal equilibrium and by employing the Vlasov equation.[12] For monotonic decreasing $f(v)$, $v^{-1}\partial f^{(0)}/\partial v < 0$ and Eq. (23) measures "energy" transfer from first order perturbation fields to the distribution function. For non-monotonic distribution functions, i.e., $v^{-1}\,\partial f^{(0)}/\partial v > 0$ for some v, there can be instability and the energy transfer in Eq. (23) is in the opposite direction.

It is important to note that $f_s^{(1)}$ and $\partial f_s^{(0)}/\partial v$ are not usually calculated in a linearized particle code, and their evaluation with any degree of precision is difficult. Numerical calculation of $(\partial f_s^{(0)}/\partial v)^{-1}$ is especially difficult. In the case that $\partial f^{(0)}/\partial v$ goes through zero and changes sign as a function of v, the division in Eq. (23) may not be well-defined. Of course, plasmas with non-monotonic $f^{(0)}(v)$ may be unstable and are therefore of particular interest. It is readily seen from the Vlasov equation, however, that if $f^{(1)}(x,v,0)$ vanishes at $v = v_c$ where $\partial f^{(0)}/\partial v$ is zero, then $f^{(1)}(x,v_c,t) \equiv 0$. Thus, it is plausible that Eq. (23) is well-behaved for non-monotonic distribution functions provided that the initial data $f^{(1)}(x,v,0)$ vanishes at the zeros of $\partial f^{(0)}/\partial v$. However,

whether a numerical calculation of Eq. (23) in a simulation would be well-behaved remains a serious question.

In two- or three-dimensional cases when the equilibrium distribution function is a function of $\varepsilon = mv^2/2 + e\phi(\vec{x})$ alone, an analogy of Eq. (23) holds:

$$\frac{d}{dt}\left[\int d^3\vec{x}\,\frac{|\vec{E}^{(1)}|^2}{8\pi} + \frac{|\vec{B}^{(1)}|^2}{8\pi} + \sum_s \int d^3\vec{x}\,d^3\vec{v}\,\frac{\left(f_s^{(1)}\right)^2}{2\partial f_s^{(0)}/\partial\varepsilon}\right] = 0 \quad . \tag{24}$$

If $f_s^{(0)}/\partial\varepsilon$ vanishes anywhere, Eq. (24) is then subject to the same limitations on the initial data $f_s^{(1)}(\vec{x},\vec{v},0)$ as was described in the preceding paragraph.

A conserved quantity can also be derived from a Lagrangian formalism based on an extension of the Low Lagrangian.[10] In a paper by Galloway and Kim[13], the Low Lagrangian for a warm plasma and finite-amplitude electromagnetic waves is derived and generalized. The single-particle Lagrangian is given by

$$\mathscr{L}^P = \frac{1}{2}mv^2 - q(\phi - \frac{\vec{v}}{c}\cdot\vec{A}) \quad , \tag{25}$$

where $\vec{v} = d\vec{x}/dt$ and ϕ and $\vec{A}$ are the electrostatic and vector potentials, respectively. The field Lagrangian density is

$$\mathscr{L}^F = \frac{1}{8\pi}\left[\left(\nabla\phi + \frac{\partial\vec{A}}{c\partial t}\right)^2 - \left(\nabla \times \vec{A}\right)^2\right] \quad . \tag{26}$$

At this point Galloway and Kim introduced an Eulerian phase space description in preparation for averaging of the Lagrangians. To distinguish Eulerian phase space variables from the polarization variables used

elsewhere in this paper we define Galloway and Kim's variables by $(\vec{X},\vec{V}) = (\vec{X}_0 + \vec{X}_1, \vec{V}_0 + \dot{\vec{X}}_1)$. Here $\vec{X}_0$ and $\vec{V}_0$ are reference position and velocity. $\vec{X}_1 = \vec{X}_1(\vec{X}_0,\vec{V}_0,t)$ represents a small displacement of a phase space element that in the absence of perturbations would be located at $\vec{X}_0$ and have velocity $\vec{V}_0$ (see Fig. 2 in Ref. 13). $\dot{\vec{X}}_1 \equiv [(\partial/\partial t) + \vec{V}_0 \cdot (\partial/\partial\vec{X}_0) + \vec{a}_0 \cdot (\partial/\partial\vec{V}_0)]\vec{X}_1$ is the velocity perturbation, with $\vec{a}_0$ the particle acceleration in the unperturbed fields. $\vec{X}_0$ and $\vec{V}_0$ are independent fluid variables, and $\vec{X}_1$ and $\dot{\vec{X}}_1$ are dependent fluid variables. When $(\vec{X}_0, \vec{V}_0) = (\vec{x}^{(0)}, \vec{v}^{(0)})$ the functional values of $\vec{X}_1$ and $\dot{\vec{X}}_1$ coincide with the values of the polarization variables $\vec{x}^{(1)}$ and $\vec{v}^{(1)}$ introduced earlier.

Galloway and Kim obtained an approximate Lagrangian by expanding the Lagrangians $\mathscr{L}^P$ and $\mathscr{L}^F$ in perturbation expansions with respect to perturbations, $\vec{X}_1$, $\dot{\vec{X}}_1$, ϕ, and $\vec{A}_1$. The particle Lagrangian is summed over plasma particles by assuming that the plasma is distributed in an approximately continuous fashion and by converting the sum of $\mathscr{L}^P$ over particles to an integral $\int d^3X d^3V f(\vec{X},\vec{V},t)\mathscr{L}^P$ where $f(\vec{X},\vec{V},t)$ is the phase space number density. Because the number of plasma particles in a cell is conserved under perturbation,

$$d^3X\, d^3V\, f(\vec{X},\vec{V},t) = d^3X_0 d^3V_0 f_0(\vec{X}_0,\vec{V}_0) \quad ,$$

where $f_0(\vec{X}_0,\vec{V}_0)$ is the equilibrium phase space number density. Neither $f_0(\vec{X}_0,\vec{V}_0)$ nor the equilibrium fields $\vec{E}_0$ and $\vec{B}_0$ is time dependent. The system Lagrangian at second order in perturbation quantities is equal to

$$L_2 = \int d^3X_0 d^3V_0 f_0(\vec{X}_0,\vec{V}_0)\mathscr{L}_2^P + \int d^3X \mathscr{L}_2^F \quad , \tag{27a}$$

where

$$\mathscr{L}^P_2 = \frac{1}{2} m \dot{\vec{X}}_1^2 - q\left\{(\vec{X}_1 \cdot \nabla)\phi_1 + \frac{1}{2}(\vec{X}_1\vec{X}_1 : \nabla\nabla)\phi_0 - \frac{\vec{V}_0}{c} \cdot \left[(\vec{X}_1 \cdot \nabla)\vec{A}_1 + \frac{1}{2}(\vec{X}_1\vec{X}_1 : \nabla\nabla)\vec{A}_0\right]\right.$$
$$\left. - \frac{\dot{\vec{X}}_1}{c} \cdot \left[\vec{A}_1 + (\vec{X}_1 \cdot \nabla)\vec{A}_0\right]\right\} \qquad (27b)$$

and

$$\mathscr{L}^F_2 = \frac{1}{8\pi}\left[\left(\nabla\phi_1 + \frac{\partial \vec{A}_1}{c\partial t}\right)^2 - \left(\nabla \times \vec{A}_1\right)^2\right] = \frac{E_1^2}{8\pi} - \frac{B_1^2}{8\pi} \quad . \qquad (27c)$$

Introduction of the action, $I_2 = \int dt\, L_2(t)$, and setting its variation equal to zero, $\delta I_2 = 0$, lead to Euler-Lagrange equations that are the equations of motion for the first order plasma displacement and electromagnetic fields:[13]

$$0 = \delta I_2 = \int_{t_1}^{t_2} dt\, \delta L_2(t) = \int d^3X_0 d^3V_0 f_0 \left(\delta\vec{X}_1 \cdot \frac{\partial \mathscr{L}^P_2}{\partial \dot{\vec{X}}_1}\right)\Bigg|_{t_1}^{t_2}$$
$$+ \int d^3X_0 d^3V_0 f_0 \int_{t_1}^{t_2} dt\, \delta\vec{X}_1 \cdot \left[\frac{\partial \mathscr{L}^P_2}{\partial \vec{X}_1} - \frac{d}{dt}\left(\frac{\partial \mathscr{L}^P_2}{\partial \dot{\vec{X}}_1}\right)\right] \qquad (28)$$
$$- \int d^3X_0 \int_{t_1}^{t_2} dt\, \delta\phi_1 \left[\nabla \cdot \left(\frac{\partial \mathscr{L}^F_2}{\partial \nabla\phi_1}\right) + \int d^3V_0\, \nabla \cdot \left(f_0 \frac{\partial \mathscr{L}^P_2}{\partial \nabla\phi_1}\right)\right]$$
$$- \int \frac{d^3X_0}{4\pi} \int_{t_1}^{t_2} dt\, \delta\vec{A}_1 \cdot \left[\nabla \times \vec{B}_1 - \frac{\partial \vec{E}_1}{c\partial t} - \frac{4\pi}{c}\int d^3V_0 f_0 \frac{\partial \mathscr{L}^P_2}{\partial \vec{A}_1}\right]$$

The variations $\delta\vec{X}_1$, $\delta\phi_1$ and $\delta\vec{A}_1$ vanish at the endpoints $t = t_1$ and t_2, but are otherwise independent and arbitrary functions. Hence, to satisfy $\delta I_2 = 0$ each of the square brackets in Eq. (28) must vanish separately, which then yields the Euler-Lagrange equations.[13]

We have derived a conservation law from the Galloway and Kim Lagrangian by using the fact that L_2 in Eq. (27) has no explicit time dependence. We consider variations induced by an infinitesimal time translation, $t \to t + \Delta t$, so that $\delta\vec{X}_1 = \Delta t(\partial\vec{X}_1/\partial t)$ [the variations need not vanish at $t = t_1$ and t_2 in Eq. (28)]. If the unperturbed orbits and fields are constrained to satisfy the Euler-Lagrange equations, then

$$\delta I_2 = \int_{t_1}^{t_2} dt\ \delta L_2 = \Delta t \int_{t_1}^{t_2} dt\ \frac{dL_2}{dt} = \Delta t \left[L_2(t_2) - L_2(t_1)\right]$$

$$= \Delta t \int d^3X_0 d^3V_0 f_0\ (\vec{X}_0, \vec{V}_0)\ \frac{\partial\vec{X}_1}{\partial t} \cdot \frac{\partial \mathscr{L}_2^P}{\partial \dot{\vec{X}}_1}\Bigg|_{t_1}^{t_2} ,$$

which upon rearranging terms allows us to identify an energy-like conserved quantity E_2,

$$E_2 \equiv \int d^3X_0 d^3V_0 f_0(\vec{X}_0, \vec{V}_0) m\ \frac{\partial\vec{X}_1}{\partial t} \cdot \dot{\vec{X}}_1 - L_2 = \text{constant}, \tag{29}$$

where L_2 is given by Eq. (27). It is important to note that E_2 is not the second order system energy and that E_2 is not composed of only positive-definite quantities.

It is illuminating to consider an example of the conservation law, Eq. (29). For Langmuir waves in a one-dimensional homogeneous plasma with $\phi_1(x) \equiv \tilde{\phi}_1 \exp(-i\omega t + ikX) + \text{c.c.}$,

$$\ddot{X}_1 = \left(\frac{\partial}{\partial t} + V_0 \frac{\partial}{\partial X_0}\right)^2 X_1 = \frac{e}{m_e} E_1 = -\frac{e}{m_e} \frac{\partial}{\partial X_0} \phi_1 ,$$

from which it follows that

$$X_1 = \frac{ike}{m_e(\omega - kV_0)^2}\,\tilde{\phi}_1 \exp(-i\omega t + ikX_0) + c.c.$$

$$\dot{X}_1 = \left(\frac{\partial}{\partial t} + V_0\,\frac{\partial}{\partial X_0}\right)X_1 \tag{30}$$

$$\frac{\partial X_1}{\partial t} = \frac{ke\omega}{m_e(\omega - kV_0)^2}\,\tilde{\phi}_1 \exp(-i\omega t + ikX_0) + c.c. \quad .$$

The dispersion relation follows from Poisson's equation,

$$1 = \frac{4\pi e^2}{m_e}\int dV_0\,\frac{f_0(V_0)}{(\omega - kV_0)^2} = \frac{4\pi e^2}{m_e k}\int dV_0\,\frac{\partial f_0}{\partial V_0}\,\frac{1}{(\omega - kV_0)} \quad . \tag{31}$$

For $\omega = \omega_r + i\gamma$, the real and imaginary parts of the dispersion relation yield

$$1 = \frac{4\pi e^2}{m_e}\int dV_0 f_0(V_0)\,\frac{(\omega_r - kV_0)^2 - \gamma^2}{\left[(\omega_r - kV_0)^2 + \gamma^2\right]^2} \tag{32a}$$

and

$$0 = \int dV_0 f_0(V_0)\,\frac{2\gamma(\omega_r - kV_0)}{\left[(\omega_r - kV_0)^2 + \gamma^2\right]^2} \quad . \tag{32b}$$

We substitute the results of Eq. (30) in Eq. (29) and average over a spatial wavelength $\lambda = 2\pi/k$ to obtain

$$\left\langle E_2 \right\rangle = \frac{k^2e^2}{m_e}\,|\tilde{\phi}_1|^2 e^{2\gamma t}\int dV_0 f_0(V_0)\,\frac{2\omega_r(\omega_r - kV_0)}{\left[(\omega_r - kV_0)^2 + \gamma^2\right]^2} \quad .$$

This is proportional to the imaginary part of the dispersion relation Eq. (32b) and therefore vanishes. Thus, despite the possible growth or damping of the Langmuir wave, E_2 is zero and is indeed conserved.

Equation (29) differs markedly in philosophy from our Poynting theorem, Eq. (22). In the Galloway and Kim approach the plasma is conceived to be a continuous Vlasov fluid, while our computational plasma is an ensemble of discrete particles. Calculation of $f_0(\vec{X}_0,\vec{V}_0)$ and $\partial\vec{X}_1/\partial t$ in a linearized particle simulation would require a phase-space grid. While the sum of the particles at all velocities within a spatial grid cell is large enough to insure adequate statistics in particle codes, if phase space were additionally subdivided into velocity bins there would typically be very few particles in each cell. The $f_0(\vec{X}_0,\vec{V}_0)$ calculated in the simulation would then only be approximately time independent because of the significant statistical fluctuations in the number of particles wandering in and out of the phase-space cell. The quantity $\partial\vec{X}_1/\partial t$ or $[\vec{V}_0 \cdot (\partial/\partial\vec{X}_0) + \vec{a}_0 \cdot (\partial/\partial\vec{V}_0)]\vec{X}_1$ would require finite differences of $\vec{X}_1$ determined locally in phase space and would also be difficult to calculate accurately because of statistical problems. It is therefore our conclusion that Eq. (29) is an interesting and valuable analytical result, but it does not lead (at present) to a practical particle code diagnostic. Equation (23), its generalization Eq. (24), and Eq. (29) are much more practical as diagnostics in simulations in which the linearized Vlasov or drift-kinetic equation is solved directly for $f_1(\vec{x},\vec{v},t)$.

Although Eq. (22) does not provide a conserved quantity, as do Eqs. (23), (24), and (29), it possesses certain essential advantages that lead us to recommend its use as a diagnostic in a particle code. Equation (22), or its time integral, contains quantities that are readily available in a linearized particle code and is easily calculable with good precision. Furthermore, the breakdown of the right side of Eq. (22) into three terms

affords valuable diagnostic information on the energy flow in and out of the first-order quantities and checks the accuracy of the solution of both Maxwell's equations and the particle equations of motion.

IV. COLD FLUID LIMIT

In the cold fluid limit, all particles within the immediate neighborhood of a field position $\vec{x}$ are presumed to share the same $\vec{x}_i^{(1)}$, $\vec{v}_i^{(0)}$, and $\vec{v}_i^{(1)}$. At a finite distance away, these values may differ due to finite spatial gradients, but they are independent of particle index. Then it follows that the linearized perturbed number density becomes

$$n^{(1)} = -(\partial/\partial\vec{x}) \cdot \sum_i \vec{x}_i^{(1)} \delta(\vec{x} - \vec{x}_i^{(0)}) = -(\partial/\partial\vec{x}) \cdot \vec{x}^{(1)} \sum_i \delta(\vec{x} - \vec{x}_i^{(0)})$$

$$= -(\partial/\partial\vec{x}) \cdot (n_0 \vec{x}^{(1)}) \quad , \qquad (33a)$$

and the current density is similarly given by

$$\vec{J}^{(1)}/e = n_0 \vec{v}^{(1)} - (\partial/\partial\vec{x}) \cdot (n_0 \vec{x}^{(1)} \vec{v}^{(0)})$$

$$= (\partial/\partial t)(n_0 \vec{x}^{(1)}) + (\partial/\partial\vec{x}) \times (n_0 \vec{x}^{(1)} \times \vec{v}^{(0)}) \quad . \qquad (33b)$$

These expressions agree with those found in Refs. 6 and 7. Bobroff, Haus, and Klüver pursued this type of analysis further and derived a small-signal power theorem of the form $(\partial/\partial t)W + (\partial/\partial\vec{x}) \cdot \vec{S} = 0$ for a cold continuum fluid, Eqs. (4.11) and II.7) of Ref. 7. Our Eq. (22) and the energy conservation law, Eq. (29), obtained from the Galloway and Kim

formalism can be shown to be mathematically equivalent to the power theorem of Bobroff, Haus, and Klüver[7] in the cold fluid limit.

In subsequent papers[14] Bobroff examined energy conservation for plasma models based on the Vlasov equation and on a model of a system composed of many cold beams. The Vlasov model gave the result presented in Eq. (23), but the beam model is rather different and interesting. Consider N beams with number densities and velocities n_i, $\vec{u}_i$, i = 1, 2, ...N and an electric field $\vec{E}$ each of which satisfy

$$\frac{\partial n_i}{\partial t} + \nabla \cdot (n_i \vec{u}_i) = 0$$

$$\frac{\partial \vec{u}_i}{\partial t} + (\vec{u}_i \cdot \nabla)\vec{u}_i = \left(\frac{e}{m}\right)_i \vec{E}$$

$$\frac{\partial E}{\partial t} + 4\pi \sum_{i=1}^{N} e_i n_i \vec{u}_i = 0 \quad .$$

If this system is linearized about an equilibrium $n_i^{(0)}$, $\vec{u}_i^{(0)}$, $\vec{E}^{(0)}$ and the equations for the first order perturbations $n_i^{(1)}$, $\vec{u}_i^{(1)}$, $\vec{E}^{(1)}$ are deduced, then there results the energy conservation law

$$\begin{aligned} \frac{\partial}{\partial t}\left[\frac{|\vec{E}^{(1)}|^2}{8\pi} + \sum_i m_i\left(n_i^{(1)}\vec{u}_i^{(0)} \cdot \vec{u}_i^{(1)} + \frac{1}{2} n_i^{(0)}\vec{u}_i^{(1)} \cdot \vec{u}_i^{(1)}\right)\right] \\ + \nabla \cdot \sum_i m_i\left(n_i^{(0)}\vec{u}_i^{(1)} + n_i^{(1)}\vec{u}_i^{(0)}\right)\vec{u}_i^{(0)} \cdot \vec{u}_i^{(1)} \qquad (34) \\ = \sum_i m_i\left(n_i^{(1)} \nabla \times \vec{u}_i^{(1)} - n_i^{(1)} \nabla \times \vec{u}_i^{(0)}\right) \cdot \left(\vec{u}_i^{(1)} \times \vec{u}_i^{(0)}\right) \end{aligned}$$

Thus, for a one-dimensional system the right side vanishes and a true conservation law is obtained, as was calculated by Bobroff.[14] It is also

evident from this generalization of Bobroff's analysis to beams in two- or three-dimensional systems that there is a conserved quantity only for irrotational flows; otherwise, Eq. (34) is in the form of a Poynting theorem.

V. EXAMPLE: MAGNETIZED ELECTROSTATIC HYBRID CODE IN CYLINDRICAL POLAR COORDINATES

In this section we consider an example that illustrates the calculations of the preceding sections. Byers[15] has developed a linearized electrostatic code which solves the Poisson equation,

$$-\nabla^2\phi^{(1)} = -\frac{1}{r}\frac{\partial}{\partial r}\left(r\frac{\partial\phi^{(1)}}{\partial r}\right) - \frac{1}{r^2}\frac{\partial^2\phi^{(1)}}{\partial\theta^2}$$

$$= -\frac{\partial^2}{\partial r^2}\phi^{(1)} - \frac{1}{r}\frac{\partial\phi^{(1)}}{\partial r} + \frac{m^2}{r^2}\phi^{(1)} = 4\pi e\left(n_i^{(1)} - n_e^{(1)}\right) , \qquad (35)$$

and advances the trajectories of particle ions self-consistently in an applied magnetic field $\vec{B} = B_0\hat{z}$. The first-order electrostatic potential, the derived electric fields, and the charge desnities are assumed to vary as $\phi = \tilde{\phi}(r,t)\exp im\theta + c.c.$ where $\tilde{\phi}(r,t)$ is a complex amplitude.

The electron fluid response is given in the low-frequency approximation ($\partial/\partial t << eB_0/m_e c$) with the electron polarization drift assumed negligible,

$$\frac{\partial\tilde{n}_e^{(1)}}{\partial t} = -\frac{im}{r}\frac{c\tilde{\phi}^{(1)}}{B_0}\frac{\partial n^{(0)}}{\partial r} \qquad (36)$$

Because Eq. (36) gives an expression for $\partial\tilde{n}_e/\partial t$, Byers' code in fact determines the electrostatic potential by using the time-derivative of Poisson's equation, Eq. (35). Derivatives with respect to r are represented

on a uniform radial grid as

$$\left[\frac{\partial^2}{\partial r^2}\,\phi^{(1)}\right]_j = \frac{\phi_{j+1}^{(1)} - 2\phi_j^{(1)} + \phi_{j-1}^{(1)}}{2\Delta r^2} \quad ,$$

$$E_{r,j}^{(1)} = -\left[\frac{\partial}{\partial r}\,\phi^{(1)}\right]_j = -\frac{\phi_{j+1}^{(1)} - \phi_{j-1}^{(1)}}{2\Delta r} \quad ;$$

and

$$E_{\theta,j}^{(1)} = -\frac{\partial}{r_j \partial\theta}\,\phi_j^{(1)} = -\frac{im}{r_j}\,\phi_j^{(1)}$$

where j is the spatial grid index.

The equilibrium is axisymmetric and trivial in the $\beta = 0$ limit (β = plasma pressure/magnetic pressure): $\vec{E}^{(0)} = 0$, B_0 is uniform and constant, and the ions execute simple cyclotron motion in the (r,θ) plane. In the presence of electric field perturbations, the zero and first order trajectories are described by the solutions of Eqs. (10) and (11). In this case z is a completely ignorable coordinate, and we set $z^{(0)} \equiv \xi_z \equiv v_z^{(0)} \equiv v_z^{(1)} \equiv 0$ for all ions. The ion equations of motion are

$$\frac{d}{dt}\,\vec{v}^{(0)} = \frac{e}{m_i c}\,\vec{v}^{(0)} \times \vec{B} \tag{37}$$

at lowest order and

$$\frac{d}{dt}\,\vec{v}^{(1)} = \frac{e}{m_i}\left(\vec{E}^{(1)} + \frac{\vec{v}^{(1)} \times \vec{B}}{c}\right) \tag{38}$$

at first order. The right sides of Eqs. (37) and (38) are evaluated at the lowest order ion position $\vec{x}^{(0)}$. This requires interpolation from the radial grid to the particle, for which linear cloud-in-cell interpolation is used.[9] The particle equations of motion are integrated using a centered leap-frog scheme.[3,9]

An essential simplification results from the axisymmetry of the equilibrium and the $\exp(im\theta)$ variation of the first order electric field. All ions at the same radius and same velocity vector (v_r, v_θ) have the same zero order trajectory except for time-independent displacements $\Delta\theta$. These in turn only lead to multiplicative factors $\exp(im\Delta\theta)$ in the first order velocities and positions. Therefore, a complete angular distribution of particles need not be tracked. It is sufficient to follow one particle per 2π radians if complex-valued amplitudes are used to represent all first order quantities. However, it is convenient here in our formal manipulations to replace the single super-particle by a continuous angular distribution of point particles at each radius.

The ion number density perturbation is

$$n_i^{(1)} = -(\partial/\partial\vec{x}) \cdot \sum_i (\xi_r \hat{r}_0 + \xi_\theta \hat{\theta}_0)_i \quad \frac{\delta(r - r_i^{(0)})}{r} \delta(\theta - \theta_i^{(0)}) , \qquad (39)$$

where $(\partial/\partial\vec{x}) \cdot = [\hat{r}\, r^{-1}(\partial/\partial r)r + \hat{\theta} r^{-1}(\partial/\partial\theta)]\cdot$. The grid representation $S(r - r_i^{(0)})$ replaces $\delta(r - r_i^{(0)})$, $\partial/\partial\theta = im$, and $(\partial/\partial r)$ is evaluated on the grid in the code. The summation on particles in Eq. (39) is performed to generate a grid quantity before the divergence is calculated. The first order current density is determined in Eq. (13),

$$\vec{J}^{(1)} = e\frac{\partial}{\partial t}\sum_i \left(\xi_r \hat{r}_0 + \xi_\theta \hat{\theta}_0\right)_i \frac{\delta\left(r - r_i^{(0)}\right)}{r}\,\delta\left(\theta - \theta_i^{(0)}\right) \tag{40}$$

$$+ e\frac{\partial}{\partial \vec{x}} \times \sum_i \hat{z}\left(\xi_r v_\theta^{(0)} - \xi_\theta v_r^{(0)}\right)_i \frac{\delta\left(r - r_i^{(0)}\right)}{r}\,\delta\left(\theta - \theta_i^{(0)}\right) \quad ,$$

where $(\partial/\partial\vec{x})x = [\hat{r}(\partial/\partial r) + \hat{\theta}r^{-1}(\partial/\partial\theta)]x$. The expressions for $n^{(1)}$ and $\vec{J}^{(1)}$ given in Eqs. (39) and (40) obviously satisfy the continuity equation.

The Poynting theorem, Eq. (22), is simple for this system,

$$\frac{d}{dt}\left(\sum_i \frac{1}{2} m v_i^{(1)2} + \int d^3x \frac{E^{(1)2}}{8\pi}\right) = -\int d^3x \vec{E}^{(1)} \cdot \vec{J}_e^{(1)}$$

$$-\sum_i e\vec{v}_i^{(0)} \cdot \left(\vec{x}_i^{(1)} \cdot \frac{\partial}{\partial \vec{x}}\right)\vec{E}^{(1)}\Big|_{\vec{x}_i^{(0)}} \tag{41}$$

where $\vec{v}_i^{(0)} = (v_r^{(0)}\hat{r}_0 + v_\theta^{(0)}\hat{\theta}_0)_i$ and

$$\hat{r}_0 \cdot \left(\vec{x}^{(1)} \cdot \frac{\partial}{\partial \vec{x}}\right)\vec{E}^{(1)} = \xi_r \frac{\partial}{\partial r} E_r^{(1)} + \xi_\theta \frac{\partial}{r\partial\theta} E_r^{(1)} - \frac{\xi_\theta}{r} E_\theta^{(1)} \tag{42a}$$

$$\hat{\theta}_0 \cdot \left(\vec{x}^{(1)} \cdot \frac{\partial}{\partial \vec{x}}\right)\vec{E}^{(1)} = \xi_r \frac{\partial}{\partial r} E_\theta^{(1)} + \xi_\theta \frac{\partial}{r\partial\theta} E_\theta^{(1)} + \xi_\theta \frac{E_r^{(1)}}{r} \quad . \tag{42b}$$

Because electron inertia is neglected, $\vec{E}^{(0)} = 0$, and only the electron $\vec{E} \times \vec{B}$ response is retained, there is no electron contribution to Eq. (41), i.e., $\vec{E} \cdot \vec{J}_e = 0$. Furthermore, for this system it is easily shown from Eqs. (7) and (20) that the ion contribution to the right side of Eq. (41) is equivalent to $-\int d^3x\, \vec{E}^{(1)} \cdot \left[\vec{J}_i^{(1)} - e\sum_i \vec{v}_i^{(1)}\,\delta(\theta - \theta_i^{(0)})\,\delta(r - r_i^{(0)})/r\right]$, which is more easily computed in the code.

Figures 2, 3, 4, and 5 illustrate the consistency of linearized simulations with the continuity equation (16) and the Poynting theorem (41) for both stable and unstable plasmas. The first example of a stable plasma (Fig. 2) consists of a kinetic equilibrium with spatially overlapped ion orbits. The subsequent examples (Figs. 3, 4, and 5) use a plasma corresponding more to a fluid equilibrium with all particle orbits encircling $r = 0$ and satisfying conditions for a rigid rotation. In a stable plasma the amplitudes of the various normal modes are constant in time and are determined by the initial conditions. Because there is apt to be a multiplicity of frequencies for a given wavenumber, especially for an energetic plasma in a magnetic field, we should not be surprised to observe the beating of stable normal modes that is evident in our energy diagnostic (Fig. 2). In the unstable case (Figs. 4 and 5), the kinetic and electric field perturbations grow exponentially in time driven by the free energy made available by the density gradient and the ion distribution function, which is monoenergetic at any radius. The Poynting theorem diagnostic provides clear evidence of the coupling of the velolcities $\vec{v}_i^{(0)}$ to the differential change in the first order electric field associated with the first order ion displacement, $\vec{x}_i^{(1)} \cdot (\partial/\partial\vec{x})\vec{E}^{(1)}$ at $\vec{x} = \vec{x}_i^{(0)}$.

We believe that the continuity equation and the Poynting theorem provide essential diagnostic checks on the accuracy of the linearized simulations considered here and also furnish valuable insight into microscopic processes. Furthermore, we have found that these conservation laws have played a vital role in debugging and developing new linearized codes and in isolating subtle difficulties associated with nonuniform equilibria and curvilinear coordinates in particular.

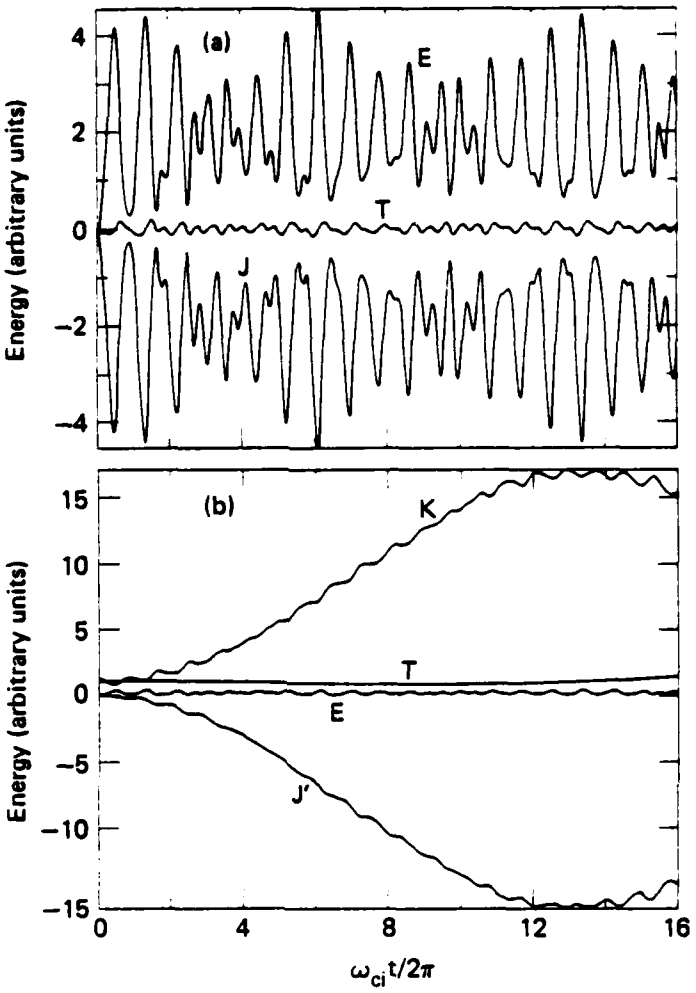

Figure 2. Linearized simulation of a stable plasma with azimuthal mode number m = 2, $\omega_{pi}^2/\omega_{ci}^2 = 1$, and density scale length $R_p = 4a$. The perpendicular velocity distribution is monoenergetic $v_\perp = a_i\omega_{ci}$, and the ion orbits overlap in space. There is a conducting wall at $r/a_i = 2$. (a) $E \equiv \int d^3x\, E^{(1)2}/8\pi$, $J \equiv \int_0^t dt' \int d^3x\, \vec{E}^{(1)} \cdot \vec{J}_i^{(1)}$, and the total energy $T \equiv E + J$ vs time. (b) $E \equiv \int d^3x\, E^{(1)2}/8\pi$, $K \equiv \sum_i (1/2)m_i v_i^{(1)2}$, $J' \equiv \int_0^t dt' \sum_i e\vec{v}_i^{(0)} [\vec{x}_i \cdot (\partial/\partial\vec{x})\, \vec{E}^{(1)}] = \int_0^t dt' \int d^3x\, \vec{E}^{(1)} \cdot [\vec{J}_i^{(1)} - e \sum_i \vec{v}_i^{(1)}\, \delta(\theta - \theta_i^{(0)})\, \delta(r - r_i^{(0)})/r]$, and the total energy $T \equiv E + K + J'$ vs time.

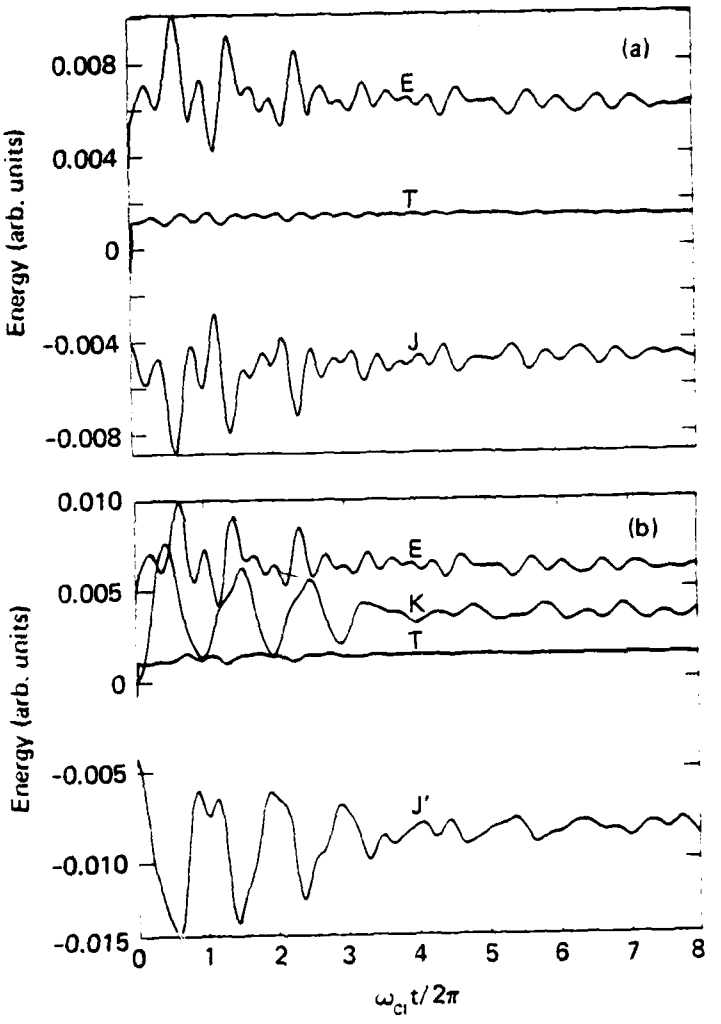

Figure 3. Linearized simulation of a stable configuration of axis-encircling ions with azimuthal mode number $m = 2$, $\omega_{pi}^2/\omega_{ci}^2 = 1$ at $r = 0$, and density profile $n_i = n_0 \exp(-r^2/r_0^2)$. The zero order trajectories satisfy $\vec{v}_i^{(0)} = -r_i^{(0)} \omega_{ci} \hat{\theta}$ where $\omega_{ci} = eB/m_i c$. There is a conducting wall at $r = 2r_0$. (a) E, J, and the total energy $T \equiv E + J$ vs time. (b) E, K, J′, and the total energy $T \equiv E + K + J'$ vs time.

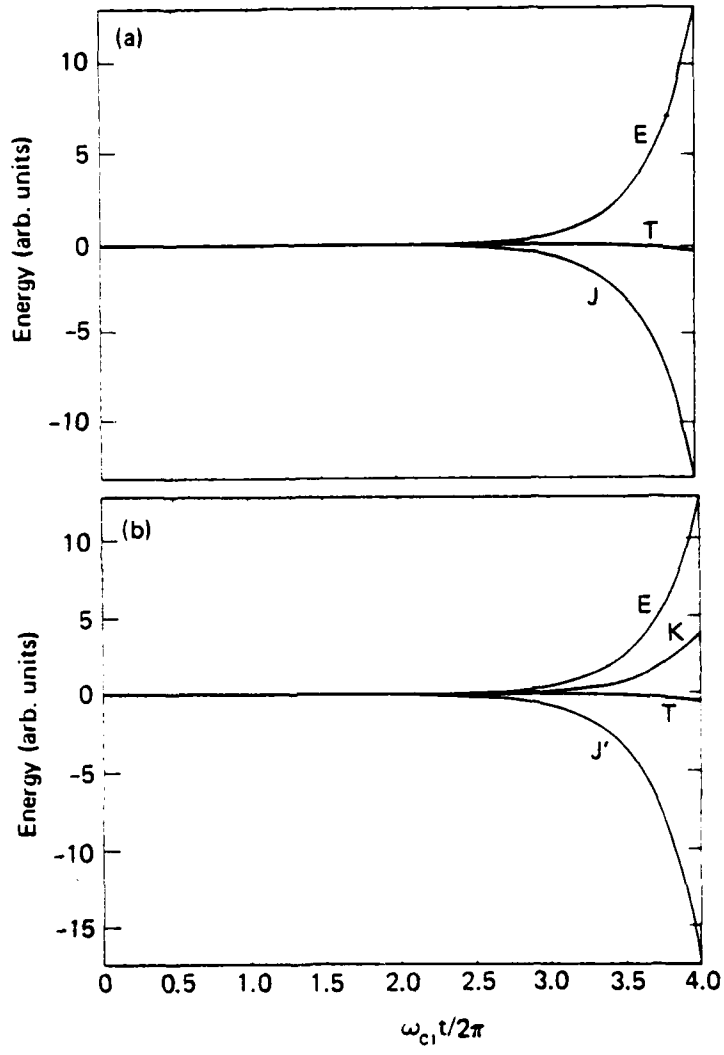

Figure 4. Linearized simulation of an unstable ($Im\omega \approx 0.2\ \omega_{ci}$) configuration of axis-encircling ions[15] with $\omega_{pi}^2/\omega_{ci}^2 = 1.5$, and otherwise the same parameters and circumstances as in Fig. 1. (a) E, J, and T = E + J vs time. (b) E, K, J´, and T = E + K + J´ vs time.

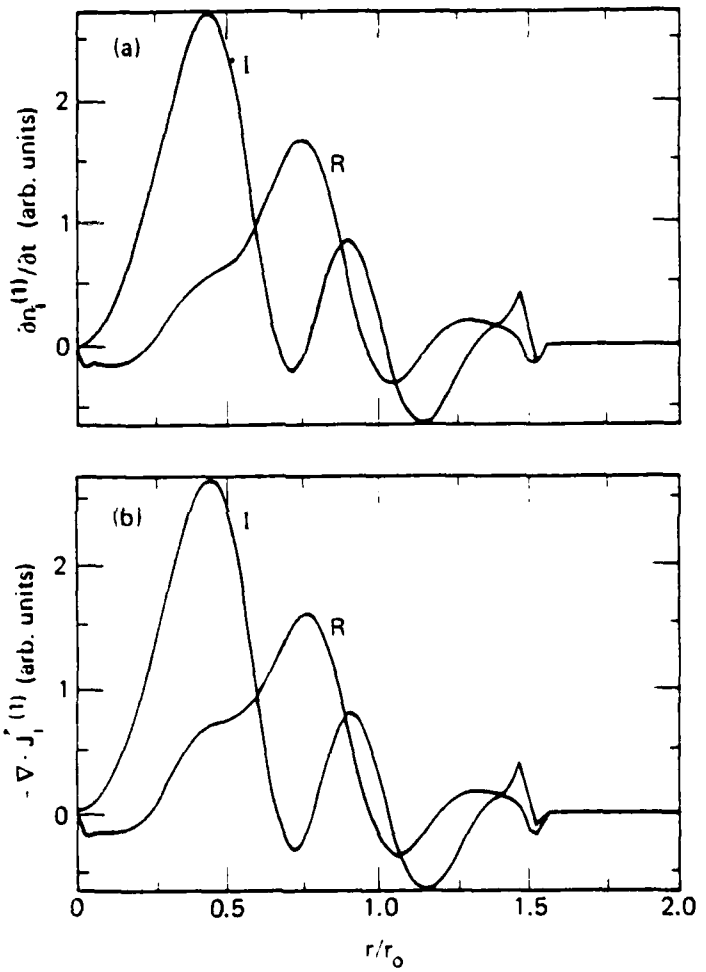

Figure 5. For the simulation described in Fig. 4, the real and imaginary parts of the complex amplitudes for $\partial n_i^{(1)}/\partial t$ and $-(\partial/\partial \vec{x}) \cdot \vec{J}_i^{(1)}$ vs r/r_0 at a particular time. The equivalence of these quantities to high degree demonstrates conservation of charge and mass.

ACKNOWLEDGMENTS

We are pleased to acknowledge and thank C. K. Birdsall, A. Friedman, Y. Matsuda, W. M. Nevins, D. Pfirsch, and J. J. Stewart for numerous discussions, assistance, and interest. This work was performed under the auspices of the U.S. Department of Energy at Lawrence Livermore Laboratory under contract No. W-7405-Eng-48.

REFERENCES

1. J. P. Freidberg, R. L. Morse, and C. W. Nielson, in "Proceedings of the Third Conference on Numerical Simulation of Plasmas," 15, Stanford University, 1969.
2. J. A. Byers, in "Proceedings of the Fourth Conference on Numerical Simulation of Plasmas" (J. P. Boris and R. Shanny, Eds.), p. 496, U.S. Government Printing Office, Washington, D.C., 1970.
3. J. A. Byers, B. I. Cohen, W. C. Condit, and J. D. Hanson, J. Comp. Phys. 27, 363 (1978).
4. A. Friedman, R. N. Sudan, and J. Denavit, "A Linearized 3-D Hybrid Code for Stability Studies of Field-Reversed Ion Rings," Cornell University LPS Rept. No. 268 (1979), submitted to J. Comp. Phys.
5. A. Friedman, Ph.D. thesis, Cornell University, 1980.
6. D. L. Bobroff, IRE Trans. PGED ED-6, 68 (1959).
7. D. L. Bobroff, H. A. Haus, and J. W. Klüver, J. Appl. Phys. 33, 2932 (1962).
8. Y. L. Klimontovich, The Statistical Theory of Nonequilibrium Processes in a Plasma (MIT Press, Cabmridge, Mass., 1967).
9. C. K. Birdsall and A. B. Langdon, Plasma Physics Via Computer Simulation (McGraw-Hill) to be published.
10. F. E. Low, Proc. Roy. Soc. A 248, 282 (1958).
11. C. Oberman and J. M. Dawson, Phys. Fluids 7, 773 (1964).
12. I. B. Bernstein, Phys. Rev. 109, 10 (1958).
13. J. J. Galloway and H. Kim, J. Plasma Physics 6, 53 (1971).
14. D. L. Bobroff, Phys. Fluids 9, 809 and 2543 (1966).

15. P. J. Catto, R. E. Aamodt, M. N. Rosenbluth, J. A. Byers, and L. D. Pearlstein, "Axis-Encircling Ion Gyro-Instability," Science Applications Report SAI-023-79-766LJ LAPS-188 (June 1979), submitted to Phys. Fluids.

F. DIGITAL FILTERING IN TIME AND HIGH FREQUENCY DAMPING

Dr. W. M. Fawley (LLL) (Prof. C. K. Birdsall)

Crystal et al. (1979) have pointed out that numerical dissipation may be inserted into plasma simulation codes by backward biasing of the field equations and/or the equations of motions. If two quantities are related by the expression, (e.g., velocity and electric field)

$$\frac{d\zeta}{dt} = \alpha(t) \tag{1}$$

Crystal et al. suggest that replacement of the usual, centered equation

$$\zeta^{n+\frac{1}{2}} - \zeta^{n-\frac{1}{2}} = \alpha^n \cdot \Delta t \tag{2}$$

by

$$\zeta^{n+\frac{1}{2}} - \zeta^{n-\frac{1}{2}} = \left(\frac{3}{4}\alpha^{n+1} + \frac{1}{4}\alpha^{n-1}\right) \Delta t \tag{3}$$

will lead to frequency-dependent numerical damping. Their algorithm has the especially nice property of the imaginary part of the computed complex frequency scaling quadratically with the normal mode frequencies (e.g., electron plasma frequency) of the system. Thus, one might introduce this dissipation in order to damp the high frequencies in the system (e.g., ω_{pe}) while keeping low frequency behavior intact, and then take much larger time steps than normal stability requirements would allow (i.e., $\omega_{pe}\Delta t > 2$).

However, the above algorithm requires implicit knowledge of quantities at times n+1 in order to advance other quantities to time $n+\frac{1}{2}$. Crystal et al. suggest implicitly solving for these advanced quantities via matrix inversion. While in principle one might attempt an iterative solution for

α^{n+1} in Eq. (3), our experience has been that, as the time step increases toward $\omega_{max}\Delta t = 2$ where ω_{max} is the maximum normal mode frequency of the system, the number of iterations necessary for a stable solution approaches infinity. Thus, we agree with Crystal et al. that an implicit solution must be used for Eq. (3) — a point made by A. B. Langdon numerous times.

Unfortunately, if α^{n+1} depends upon individual particle properties such as position, the necessary matrix inversion for implicit solution becomes impracticable. One variation of the backward-biasing present in Eq. (3) appealed to us which would minimize the need for iteration. Rather than use as large a time separation as $2\Delta t$ on the right side of Eq. (3), why not decrease this separation to $2\delta\Delta t$ with $\delta \ll 1$ as in the following set of equations:

$$v^{n+\frac{1}{2}} - v^{n-\frac{1}{2}} = \frac{q\Delta t}{m}\left(\left(\frac{1+\epsilon}{2}\right)E^{n+\delta} + \left(\frac{1-\epsilon}{2}\right)E^{n-\delta}\right) \tag{4}$$

$$= \frac{q\Delta t}{m} E^{n*}$$

$$\nabla \cdot E^{n\pm\delta} = 4\pi\rho^{n\pm\delta} \tag{5}$$

$$x^{n+1} - x^{n} = v^{n+\frac{1}{2}}\,\Delta t \tag{6}$$

where $0 \leq \epsilon \leq 1$ is the biasing factor.

The hope in using Eq. (4) is that since $v^{n-\frac{1}{2}}$ and E^{n} are known, then one can make a very accurate prediction for $E^{n\pm\delta}$ for δ small. We employed the following algorithm:

$$E^{n-\frac{1}{4}} \equiv \frac{3}{4}E^{n} + \frac{1}{4}E^{n-1} \tag{7}$$

$$v^{n} \equiv v^{n-\frac{1}{2}} + \frac{1}{2}\Delta t\,\frac{q}{m}E^{n-\frac{1}{4}} \tag{8}$$

$$x^{n\pm\delta} \equiv x^{n} \pm \delta\cdot\Delta t\cdot v^{n}\ . \tag{9}$$

The algorithm from time $(n-\frac{1}{2})$ to $(n+\frac{1}{2})$ is shown in Fig. 1. The sequence is: $E^{(n-1)*} \rightarrow v^{n-\frac{1}{2}} \rightarrow x^{n} \rightarrow E^{n} \rightarrow E^{n-\frac{1}{2}} \rightarrow v^{n} \rightarrow x^{n\pm\delta} \rightarrow E^{n*}$. The equations are time-centered except for expression (9) which deviates to first order in δ.

If one analyses this algorithm by assuming all quantities vary as $\exp(-i\omega t)$ and that the normal mode frequency is ω_o, one obtains for $\omega_o \Delta t \leq 1$ with $\varepsilon = 0.5$, $\delta = 0.2$, $\Delta t = 1.0$ (see Figs. 2 & 3),

$$\omega_r - \omega_o \approx 0.04\omega_o^3 \Delta t^2$$

$$\omega_i \approx .06\omega_o^2 \Delta t$$

i.e., the method produces frequency-dependent damping. Figures 4 and 5 show the effect on ω_r and ω_i of varying δ while keeping all other parameters constant.

Introducing the algorithm into ES1 was not difficult and the only significant additional memory requirements were supplying the array space for E^{n-1}. For $\omega_o \Delta t < 2.0$, the algorithm worked as expected in that high frequencies were damped much more than low frequencies. We also experimented with arbitrarily turning the damping on and off. One example is shown in Fig. 6 where the damping was "on" for $0 < t \leq 150$ and "off" for $t > 150$. As expected, the electrostatic energy in mode 32 exponentially damped for $t < 150$ and then remained constant for greater times.

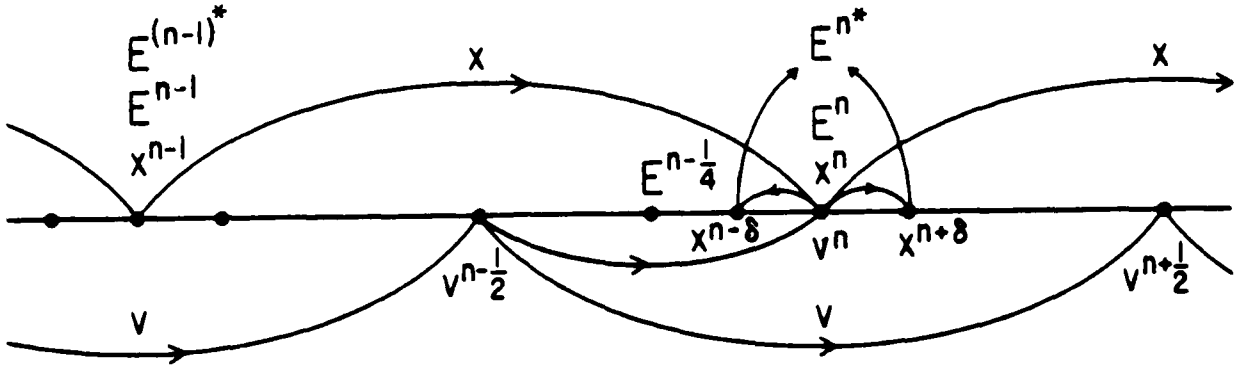

FIG. 1 Leapfrog integrator with micro ($\delta\Delta t$) and normal (Δt) time stepping, showing detail about time t^n. The micro steps are used to alternate the high frequency content up the electric field, with E^{n*} used to advance the velocity from time $n-\frac{1}{2}$ to $n+\frac{1}{2}$.

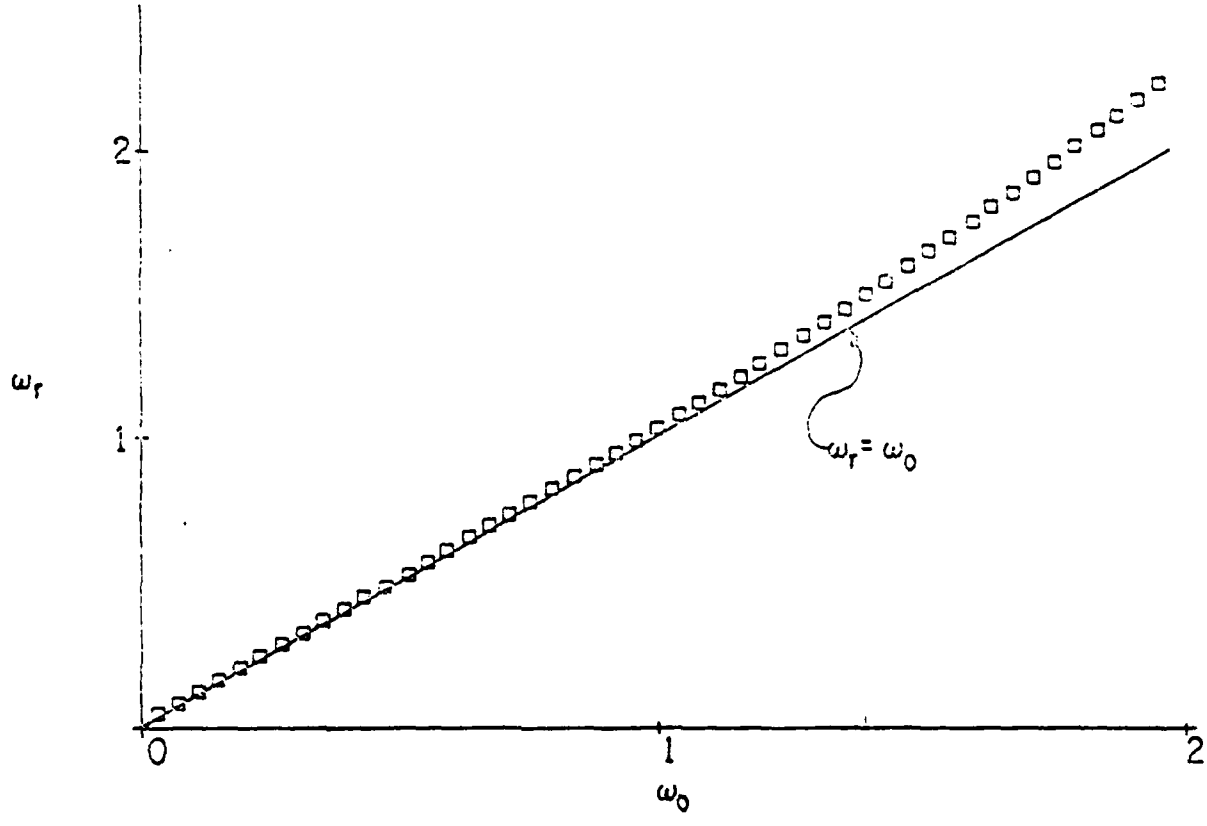

FIG. 2. The real part ω_r of the dispersion relation is plotted versus the driving frequency (e.g., ω_{pe}). Here $\Delta t = 1.0$ sec, $\varepsilon = 0.5$, and $\delta = 0.2$. The straight line $\omega_r = \omega_o$ is also shown.

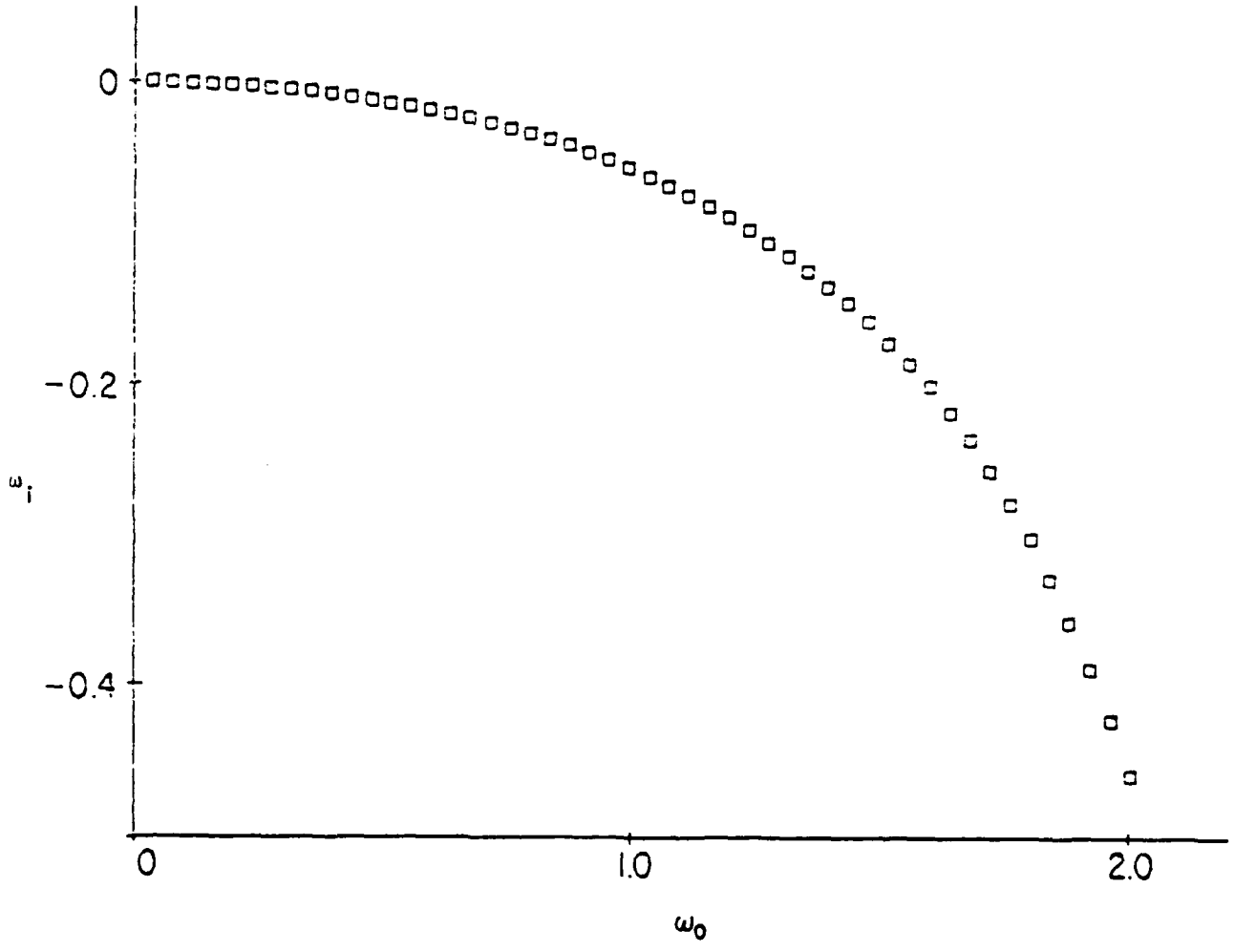

FIG. 3 The imaginary plot ω_i is plotted versus ω_o for the same parameters as in Fig. 2. Note the quadratic increase in $|\omega_i|$ with increasing ω_o which leads to preferential damping of high frequencies.

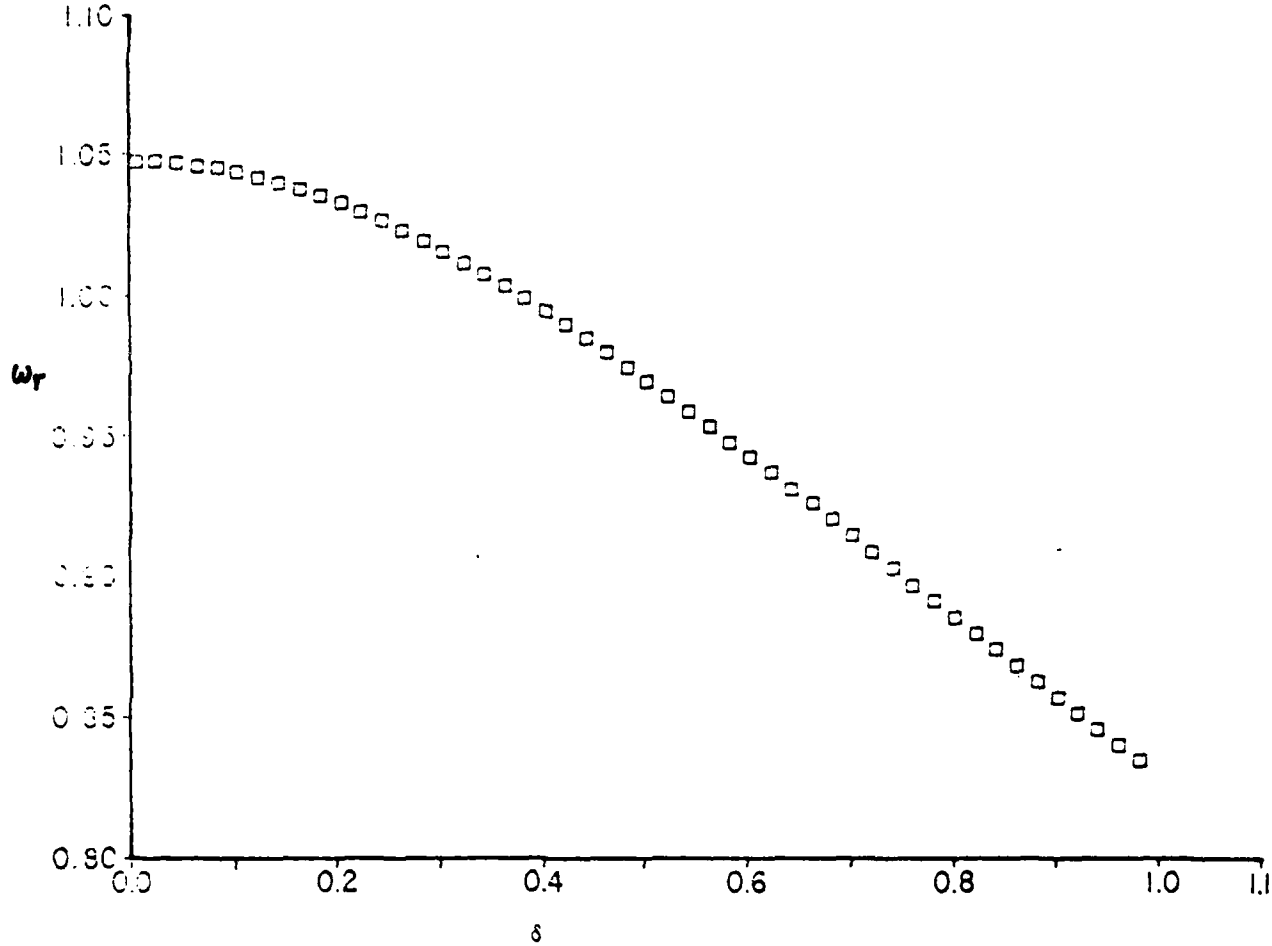

FIG. 4. Same as Fig. 2 except δ is varied and ω_o is fixed at 1.0.

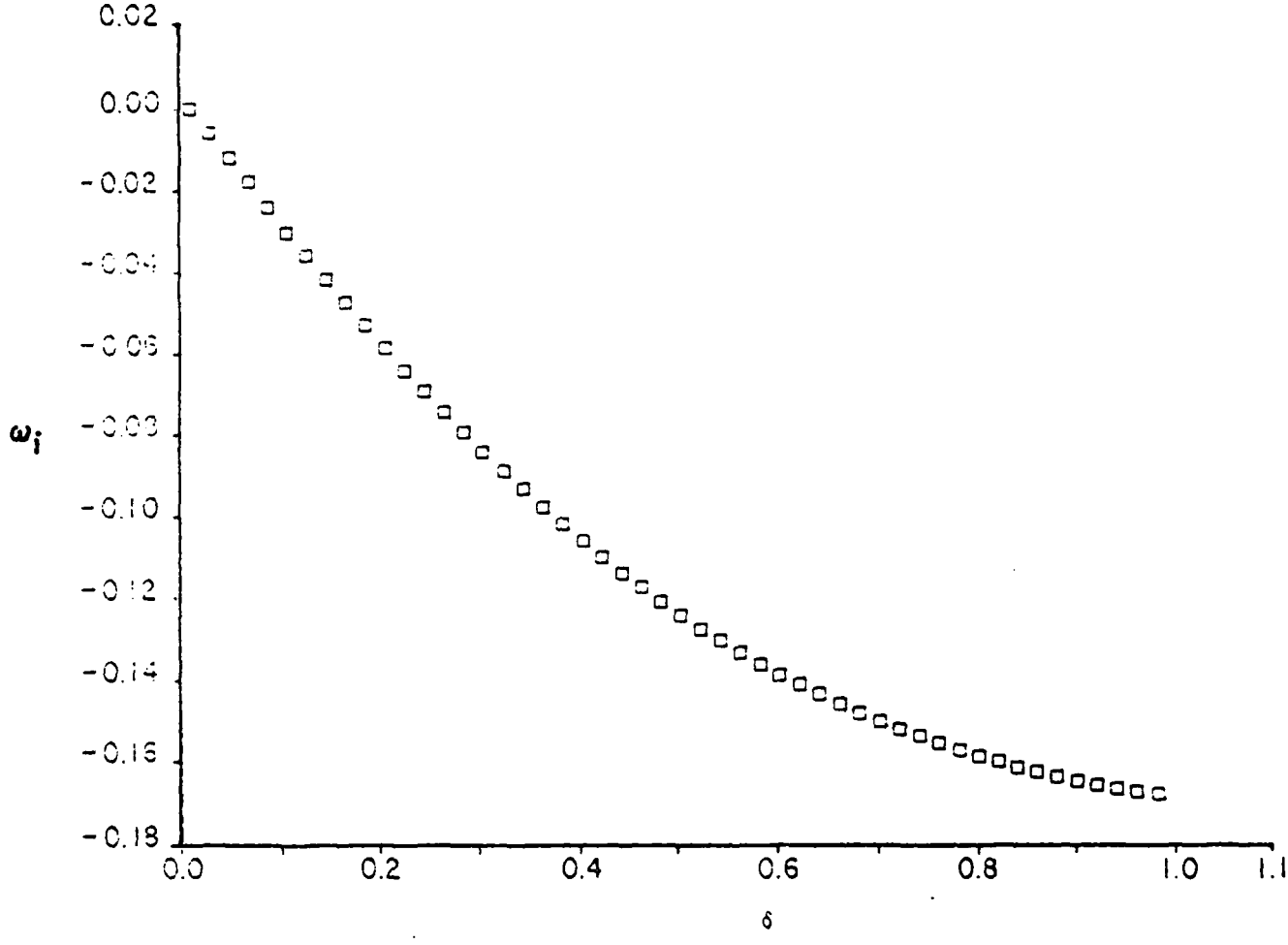

FIG. 5 Same as Fig. 3 except δ is varied and ω_o is fixed at 1.0.

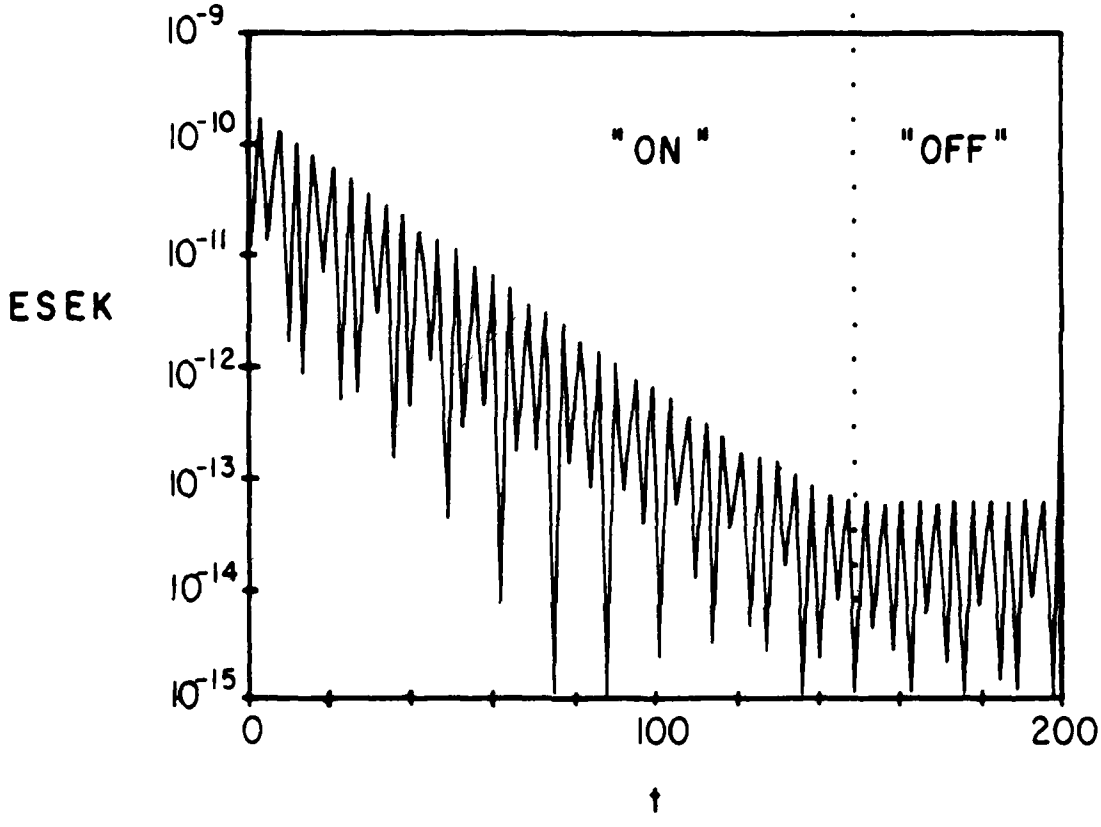

FIG. 6. The electrostatic energy is plotted (logarithmically) versus time. The damping algorithm is "on" for $0 < t \leq 150$ and is "off" for greater times. Mode 32.

Unfortunately, the algorithm is not stable for $\omega_o \Delta t \gtrsim 2.0$. The problem is probably in expression (7) where E^n should be replaced by its biased counterpart, which again requires an implicit solution. It is possible that iteration may be more useful in this algorithm than that of Crystal et al. To work around this instability problem, we experimented with the following "hybrid" time-step scheme: For each long time step ($\omega_o \Delta t_{long} > 2$) taken by the code which excites high frequency oscillations, take many (N_{short}) time steps using the algorithm above to damp out these unwanted oscillations. Normal modes with $\omega \ll 2\Delta t_{long}^{-1}$ should remain unaffected by the varied time step. In practice, we discovered the following behavior. Each long time step leads to an <u>exponential</u> growth in the electrostatic energy contained in high frequency modes and the argument of the exponential scales <u>linearly</u> with Δt_{long} (see Fig. 7). Thus, the ratio of $N_{short}\Delta t_{short}$ to $N_{long}\Delta t_{long}$ must be equal to or greater than some constant for stable behavior in all modes. For $\omega_o = 1.0$, $\Delta t_{short} = 1$, $\varepsilon = 0.5$, $\delta = 0.2$, $N_{short}\Delta t_{short}/N_{long}\Delta t_{long} \gtrsim 20$.

That is, in using this hybrid scheme one gains less than 5% in the total time simulated for a given number of time steps as compared with a normal simulation just using Δt_{short}. Therefore, unless a solution is found for the $\omega_o \Delta t > 2.0$ instability, the damping algorithm does not appear to be useful for very long time step simulations despite its simplicity of coding and frequency-dependent damping properties.

It is to be noted that we still have gained some advantage in being able to work up to $\omega_{pe}\Delta t \sim 1.5$, with damping increasing quadratically with $\omega_{pe}\Delta t$, producing the desired (undamped) physics at $\omega \ll \omega_{pe}$. The ultimate goal of being able to allow $\omega_{pe}\Delta t > 2$ still eludes us.

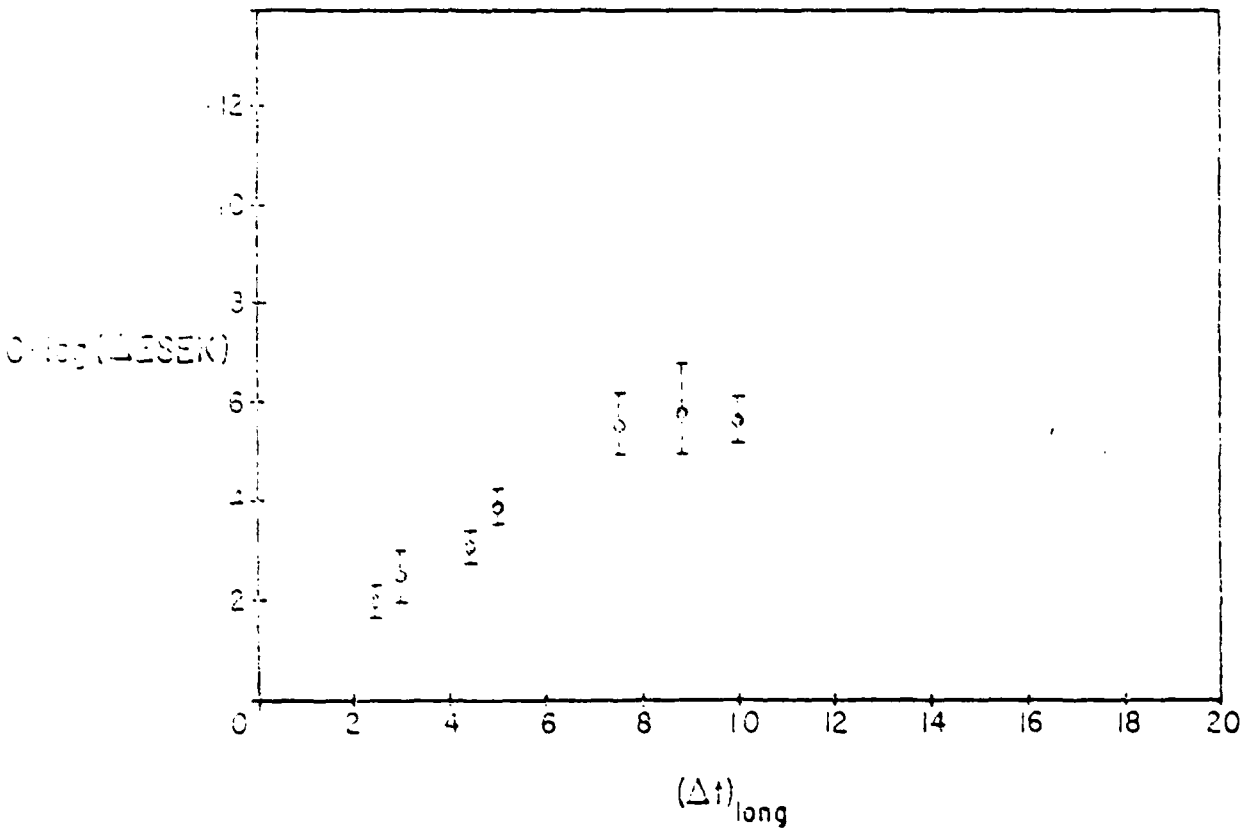

FIG. 7. The jump in the logarithm of the electrostatic energy in a given mode from taking a single time step with $\Delta t_{long} > 2\omega_o^{-1}$ is plotted versus Δt_{long}. The approximate linear relationship indicates that the number of short-time steps employing time-filtering required to damp out this jump varies directly with the length of the jump in Δt.

REFERENCES

Crystal, T. L., Denavit, J., and Rathman, C. E., Comments on Plasma Physics and Controlled Fusion. 5, 17 (1979).

Section II
CODE DEVELOPMENT and MAINTENANCE

A. ES1 CODE

No special report this quarter.

B. EM1 CODE

No special report this quarter.

C. EZOHAR CODE

No special report this quarter.

D. RINGHYBRID CODE

Alex Friedman

Several errors were made in the original implementations of the code; these have not affected results for ion rings significantly, since they are small for currents at radii large compared to the cell size, in general. For plasmas with current near the axis, such as FRM plasmas, it may be important to use the correct expressions (derived elsewhere in this report).

The first error was a failure to note the vectorial nature of the term $(\underline{\varepsilon}_k \cdot \nabla)\underline{v}_k$; due to the azimuthal derivatives of the unit vectors, two terms result:

a contribution to $J^1_{rk} \propto \varepsilon_{\vartheta k}\dot{\theta}_k$

a contribution to $J^1_{\vartheta k} \propto -\varepsilon_{\theta k} v^o_{rk}/r^o_k$.

The next error was a failure to recognize the radial variation of v_θ^o for each superparticle, necessary if there is to be no shear to the flow. The first consequence of this is the appearance of an extra term in the first-order current:

a contribution to $J_{\theta k}^1 \propto -\varepsilon_{rk}\dot{\theta}_k$.

The second consequence is that azimuthal current densities J_θ^o, J_θ^1 must be computed in a different manner than n^o:

J_θ^o: divide by $2\pi r_o$ (particle) rather than $2\pi r$ (cell).

J_θ^1: divide by $2\pi r_o$ (particle) rather than $2\pi r$ (cell) .

These changes were implemented into the code, and $\nabla\cdot\underline{J}^1$ now closely approximates $-\dot{n}^1$. Results regarding stability of ion layers and rings were not altered greatly.

E. RADIAL SIMULATION CODE ES1RB

No special report this quarter

F. RADIAL CODE NOTES (R,Rθ,RZ,RθZ)

1. Rθ Area Weighting of Charge (Method A)

C. K. Birdsall

Charges are to be weighted to an Rθ grid. Let them be rod shaped clouds with curvilinear shape Δr by $r\Delta\phi$ uniform in z as shown in Fig. 1. The grid has cells Δr by $r\Delta\phi$. The cell in which the particle appears is given inner radius r_i, outer radius r_{i+1} and angular grids ϕ_j, ϕ_{j+1}.

The coordinates of the particle r_p, ϕ_p are taken to be the arithmetic mean. The curvilinear cloud is taken to have charge q_p coulombs / m, with uniform charge density at the instant of weighting. As the area of the cloud is $(r^2_{outer} - r^2_{inner})\Delta\phi/2 = r_p \Delta r \Delta\phi$, then the density of the cloud $\begin{cases}\text{decreases}\\ \text{increases}\end{cases}$ as r_p $\begin{cases}\text{increases}\\ \text{decreases}\end{cases}$ at the next instant; no account is made for the energy $\begin{cases}\text{loss}\\ \text{gain}\end{cases}$ as the cloud $\begin{cases}\text{expands}\\ \text{contracts}\end{cases}$ in angular length.

In an axisymmetric system, with no ϕ variation there are just charged shells of thickness Δr, as in Fig. 2. Ignoring the grid, the force on shell 2 of density q_2 due to shell 1 producing field E_1 is (see Fig. 3),

$$F_r(\text{on 2 due to 1}) = \int_2 \sigma_2 E_1 \, dV \qquad \begin{matrix}(E \text{ is radial,}\\ \sigma \text{ is in Coulombs/m}^3)\end{matrix}$$

where

$$E_1 = \frac{q_1}{2\pi\epsilon_o r} \, . \qquad (q \text{ is in Coulombs/m})$$

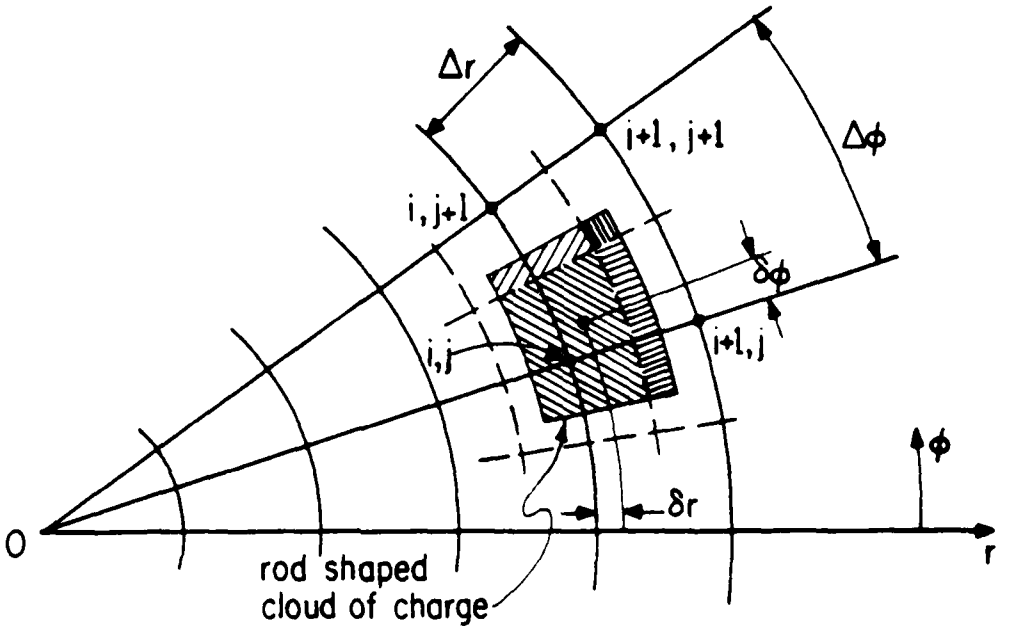

FIG. 1. Cloud of charge q, a rod parallel to z, uniform in density, located at $r_i \phi_p(\cdot)$, δr, $\delta\phi$ from grid point ij. Shaded areas are weighted to nearest grid points. The cloud shape $\dot{r}\Delta\phi$ by Δr is curvilinear, with $\Delta\phi$, Δr fixed. The grid uses the same $\Delta\phi$, Δr, fixed.

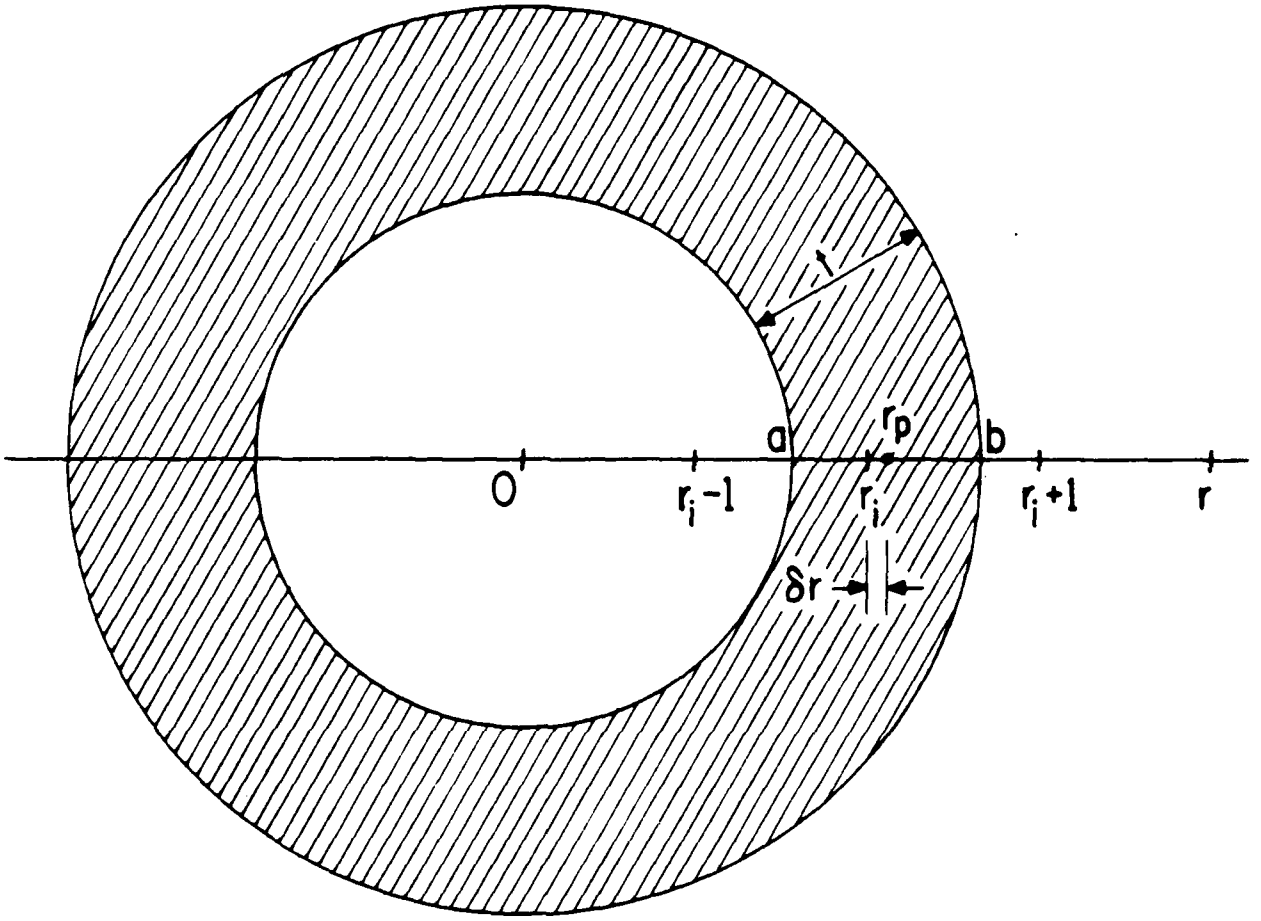

FIG. 2. Cloud shell of charge q, a cylindrical shell centered on origin 0, uniform in density, located at $(\cdot)r_p$, δr from grid point r_i. The shell is the rod of Fig. 1, with angular width $\Delta\phi$ made to be 2π; the radial width is $t = \Delta r$. For $r_p = \Delta r/2$, the inner shell radius is at $r = 0$; for $r_p < \Delta r/2$, the shell inner radius moves outward, crossing the outer radius for $r_p = 0$; that is, the shell folds through the origin.

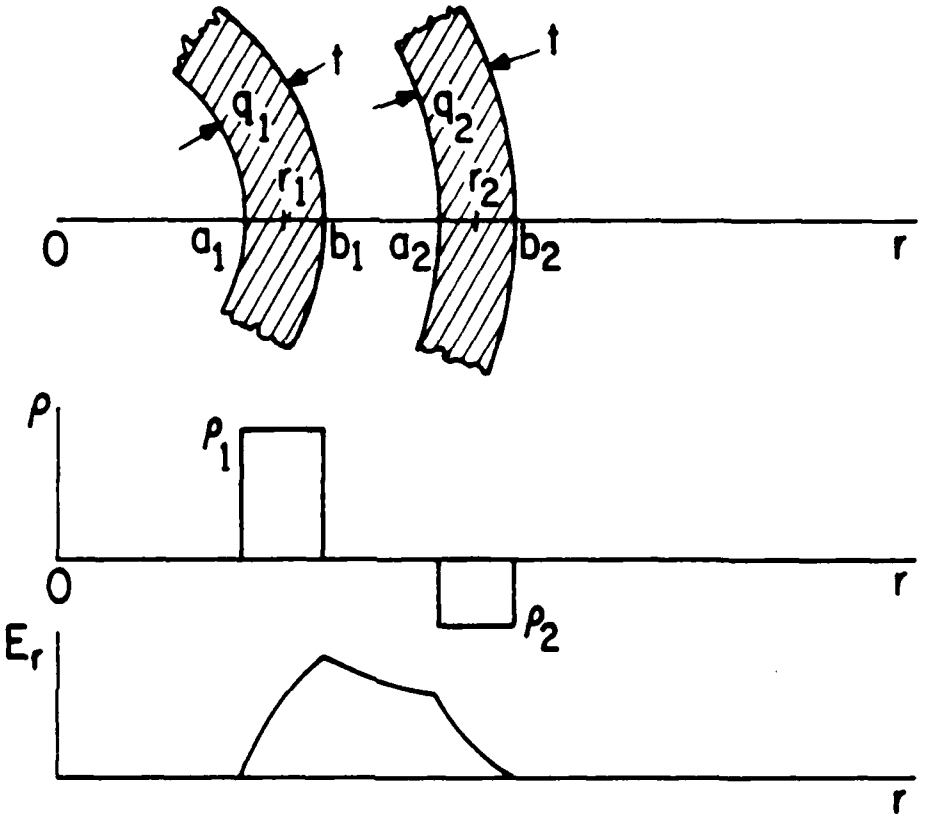

FIG. 3. Two charged cylindrical shells, taken to have constant charge density ρ within each shell, and the same charge per unit length in z, q. ρ and q are related by $q = \pi(b^2-a^2)\rho$ or $\rho = q/2\pi r_p t$. The sketches of ρ and E_r are for q_1 and $q_2 = 0$.

So

$$F_r = \int_2 \frac{q_1}{2\pi\varepsilon_o r} \rho_2 \, 2\pi r \, dr dz = \frac{q_1 \rho_2 (b-a)}{\varepsilon_o} \, dz$$

for ρ_2 independent of r. (As the particle moves, with, say, shell thickness kept constant, then within a shell ρ_i changes; the assumption here is that, at any given position, ρ is independent of r.) This expression is awkward to use as ρ_2 changes as the particle moves; this form can be improved by changing ρ_2 into a charge/length quantity which does not change as the particle moves, writing

$$q_2 = \rho_2 \pi (b^2 - a^2) = \rho_2 2\pi t \left(\frac{b+a}{2}\right) = \rho_2 2\pi t r_p \, .$$

Hence,

$$F_r(\text{on } q_2 \text{ due to } q_1 \text{ inside of } q_2) = \frac{q_1 q_2}{2\pi\varepsilon_o r_p} \quad \text{(Newtons/m)}$$

$$= q_2 E_r(\text{at } r_p \text{ due to } q_1);$$

that is, use E_r as measured at the center of the charge being moved. Of course, E_r may be due to many q_i all lying within shell q_2; simply replace q_1 above with $\sum_{i=1} q_i$. See Fig. 4 for thin shells

There is also a self-force in that a cylindrical shell tends to expand, in contrast to a planar sheet, which does not (with some exceptions, like the sheet in question not midway between sheets of opposite sign, or at $\pm\infty$, etc.) That is, a shell at r_p produces a field between itself and charge of opposite sign at $r > r_p$, such that there is a force on the shell of value $\int_{\text{shell}} \rho E dV$; this force for ρ constant over the shell (E_r is

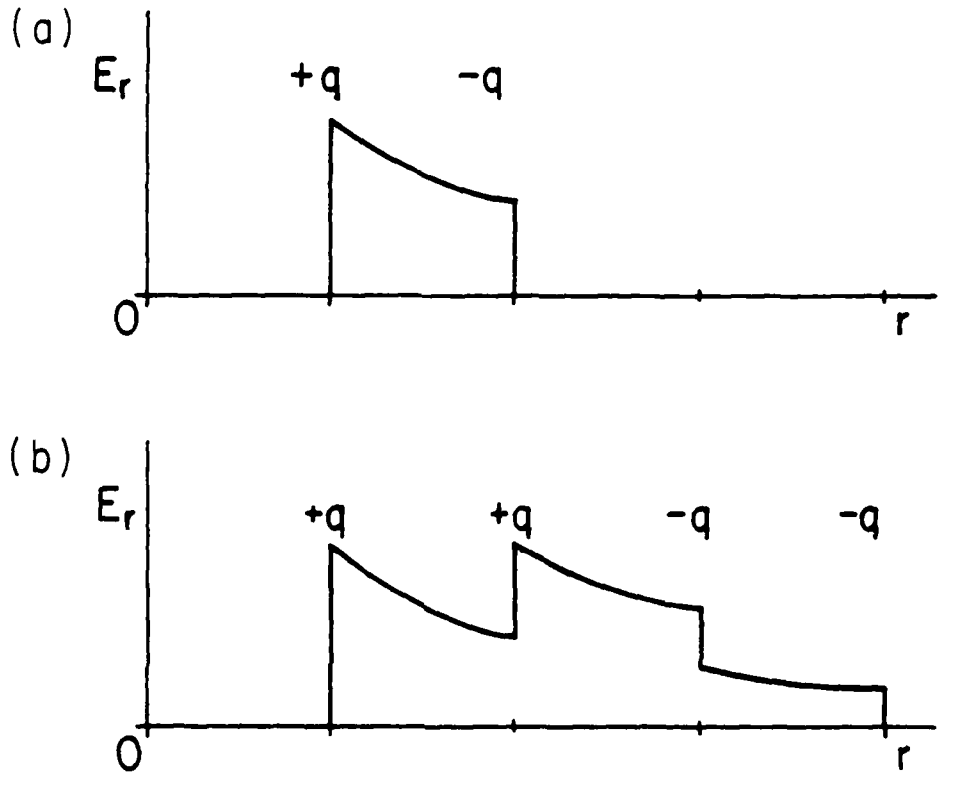

FIG. 4. Variation of E_r with neutral sets of thin charged shells. The jump in D_r is ρ_s (Coulombs/m^2) which is $q/2\pi r$. Note the contrast with planar sheet models, with the same jump at each sheet and no variation between sheets.

$\rho(r^2 - a^2)/2\varepsilon_o r)$ is,

$$F_{r_{self}} = \frac{q^2}{2\pi\varepsilon r_p}\left(\frac{a + t/3}{2r_p}\right) \quad . \qquad \text{(Newtons/m)}$$

The factor in parentheses varies from 1/3 to 1/2 as a/t varies from 0 to ∞ (from rod on axis, to thin shell). Hence, the self-force varies from 1/3 to 1/2 that of <u>one</u> shell of charge q inside the shell of interest of charge q; for many charges inside a shell, the self-force may be negligible (unless the <u>net</u> charge enclosed is comparable to q).

2. Method B

Weighting in Rθ may be done using the recipe implied in Fig. 1. This will be done straightforwardly. Then the limit $\Delta\theta \to 2\pi$ will be made, producing ring (or shell) charges and radial weighting to be compared with Method A (see QPR III for this year).

The total charge to be weighted to the nearest four grid points is q (as q is a rod, the units are Coulombs/meter). The area of an element of q of angular width α extending between r_{inner} and r_{outer} is

$$\delta(\text{area}) = \iint r\, dr d\phi = \frac{1}{2}(r_o^2 - r_i^2)\alpha = (r_{mean})(\text{width})\alpha$$

where $r_{mean} = (r_i + r_o)/2$ and $(\text{width}) = r_o - r_i$.

The fractional area to be assigned to a grid point is

$$\frac{\delta(\text{area})}{\text{total area}} = \frac{(r_{mean})(\text{width})\alpha}{r_p \Delta r \Delta\phi} \quad .$$

Using the symbols in Fig. 1, $\delta r = r_p - r_i$, $\delta\phi = \phi_p - \phi_j$, we may construct r_{mean} and width for the four grid points and hence, the weights. This is done in Table 1.

Adding all of the $[(r_{mean})(width)\alpha]$'s does indeed turn out to be $r_p \Delta r \Delta\phi$, a first check (total area or charge conserved).

For rings (or shells), let $\Delta\phi \to 2\pi$. Then the weight (a fraction of charge) assigned to r_i is q_i,

$$q_i = q\left(r_i + \frac{\delta r}{2}\right)(\Delta r - \delta r)/r_p \Delta r$$

and that assigned to r_{i+1} is q_{i+1},

$$q_{i+1} = q\left(r_i + \frac{\Delta r + \delta r}{2}\right)(\delta r)/r_p \Delta r \ .$$

We next compare these weights with Method A of QPR III, this year.

Table 1

*R-θ Area Weights**

grid point	r_{inner}	r_{outer}	r_{mean}	width	α
i,j	$r_i - \frac{\Delta r}{2} + \delta r$	$r_i + \frac{\Delta r}{2}$	$r_i + \frac{\delta r}{2}$	$\Delta r - \delta r$	$\Delta\phi - \delta\phi$
i+1,j	$r_i + \frac{\Delta r}{2}$	$r_i + \delta r + \frac{\Delta r}{2}$	$r_i + \frac{\Delta r + \delta r}{2}$	δr	$\Delta\phi - \delta\phi$
i+1,j+1	$r_i + \frac{\Delta r}{2}$	$r_i + \delta r + \frac{\Delta r}{2}$	$r_i + \frac{\Delta r + \delta r}{2}$	σr	$\delta\phi$
i,j+1	$r_i - \frac{\Delta r}{2} + \delta r$	$r_i + \frac{\Delta r}{2}$	$r_i + \frac{\delta r}{2}$	$\Delta r - \delta r$	$\delta\phi$

*$\delta r = r_p - r_i$ and $\delta\phi = \phi_p - \phi_j$

Using the subscripting of Fig. 1, with grids at r_i, r_{i+1} and particle located at r_p between r_i, r_{i+1},

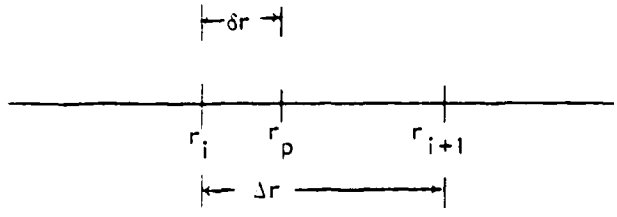

the results of Method A are

$$q_i = q(r_i)(\Delta r - \delta r)/r_p \Delta r$$

$$q_{i+1} = q(r_{i+1})(\delta r)/r_p \Delta r \ .$$

The differences are slight. Method B has the first factors as the mean of (r_i, r_p) or (r_p, r_{i+1}) where Method A has r_i, r_{i+1}. Method B is derived formally, is taken to be more accurate, and is recommended as a charge in existing codes. Be careful; note whether charge or density is being weighted.

******* ******* ******** ******** ********

These notes are being included somewhat randomly, to be collected later in a more ordered fashion, with tests, criticisms, recommendations, etc.

******* ******* ******** ******** ********

Previous QPR, Fig. 1 on Page 94 is perhaps more clearly understood if the ordinate $q(r_j)$ is replaced by $q_{r_j}(r_i)$; that is, r_i is being varied, not r_j. The particle at r_i is moving past the fixed grid point r_j.

G. RJET DEVELOPMENT

No special report this quarter

H. SOFTWARE DEVELOPMENT (RUN, SOLVER)

RUN

H. Stephen Au-Yeung and Niels Otani

Being the first entry of a LIB file, RUN executes any program within the LIB file. The purpose of having RUN is to encourage users to put their programs into a library. RUN is on the CRAY-1 computer and can be obtained by typing:

```
rfilem read 1222 .cray run(ESC) end
```

This document corresponds to the RUN version of February 11, 1980. Later versions of RUN will be stored in FILEN directory .cray of user number 1222. The user should periodically check the date of these files (rfilem now 1222 .cray run) to see if the program has been updated. The file RUN is a LIB file: it contains the latest source as well as the latest version of this documentation. To obtain this document, type:

```
lib run(ESC)x run.doc(ESC)end
netout [use] run doc [turn.] box 3nn run
```

Suppose RUN is the first entry of the LIB file ALL, which contains programs like COMOUT and FREX. As an example, the user may execute COMOUT and FREX as follows:

```
user          : all      10 !
run user      : -comout ucb endwith.  s s. box b22 source
comout user:  \end
comout        :  \comout\ : file-id is comout    - rxucb/ka
run user      : -frex f105ro0x  5 t 30  box b22 fr90file
frex          :  Processing file:     f105ro0x
run user      : -end
```

Note that ALL will not be terminated until "end" is entered after the prompt "-". If the program entered is not in the library (a public file, for example), RUN will also execute it.

SOLVER

H. Stephen Yu-Yeung

SOLVER has been updated on March 15, 1980. The new version has the following changes:

(1) SOLVER now works on the new LDR formats. For those who would like to use the old LDR may get the old version of SOLVER by typing - ...filem read 1222 .classic.solver.ESO)end ... t ... on the CRAY.

(2) A new variable, MARK, has been added to the NAMELIST read so that the user may specify the marker for the curve(s) of his/her roots or function plotting.

MARK = +i => points connected and a symbol every ith point.
-i => points not connected and a symbol at every ith point.
0 => points connected with no symbols drawn (default).

(3) Another new variable, FNREAL, has been added to the NAMELIST read to enable SOLVER to look for only pure real roots.
FNREAL = 1 => to force all approximations to all the roots to be real.
0 => allow complex roots (default).

Section III

PLASMA SIMULATION TEXT

The text is under review by McGraw-Hill.

Section IV

SUMMARY of REPORTS, TALKS, PUBLICATIONS, and VISITORS

Abstracts of papers presented at APS Division of Plasma Physics Meeting, Boston, Nov. 12-16, 1980 were given in the previous QPR.

We were pleased to have visits from Steve Gitomer (LASL) on Oct. 19 and from Mike Gerver on Dec. 5-8.

Alex Friedman presented a colloquium at the Cornell University Laboratory for Plasma Studies, Oct. 3, on "Simulation Studies of the Stability of Field Reversed Ion Rings".

Section V

INFORMAL CONFERENCE ON PARTICLE AND HYBRID CODES FOR FUSION

December 10 & 11, 1979

Napa, California

CONTENTS

ACKNOWLEDGMENTS

This conference was conceived during a telephone call with David Nelson at DOE roughly two months ago. His suggestions as to purpose and focus, as well as his active participation in the meetings are acknowledged most gratefully.

My colleague, Alex Friedman, has been invaluable in all stages of conference preparation from the suggestion of topics to be covered, and their grouping, consultation with many outside Berkeley, LBL, and LLL, the formulation of invitations, to many details of the meeting itself. I am most grateful for his help.

Ginger Pletcher, my part-time assistant, devoted nearly all of her time for two months to finding a suitable meeting place near Berkeley (but far enough away to keep participants from straying to LBL, LLL, Stanford, etc.

during the meetings) for the meetings and a pleasant place for the conference dinner. She also did the typing, letter writing, and mailing to the potential and actual participants (with help from Steve Au-Yeung on the initial computer mailing), made many phone calls to ensure that the details of the conference were handled properly, and arranged the get-together Sunday evening. We owe Ginger an immense vote of thanks for her help.

My thanks go to the speakers and panelists for their excellent presentations, which are already stimulating us to better work. The interchange of ideas that was sought was achieved; the interaction with David Nelson that was desired was also achieved.

C. K. Birdsall
Berkeley, Dec. 17, 1979

I. PURPOSE

This conference was held in order to facilitate an exchange of ideas and results on plasma particle and particle-fluid hybrid codes in an informal, unpublished manner, with frank and open discussion among about fifty people. The only printed record is the collection of copies of transparencies used by the thirty-five speakers. In keeping with this informality, the transparency copies were distributed to the participants only and are not to be quoted without explicit permission from the author.

In December 1974 we organized a similar unpublished conference in Berkeley at the request of Robert Price of ERDA. The present conference is a follow-up and is due in large part to the interest of David Nelson (Chief, Fusion Theory and Computer Services Branch, Div. Applied Plasma Physics,

Office of Fusion Energy, DOE). Dr. Nelson presented his view from DOE of contributions by computation and simulation toward furthering plasma research leading to fusion reactors; he received considerable feedback from participants. We are most grateful to him for his active and stimulating participation.

The conference is also due to the pressure of accumulated interest among those who work with particle and hybrid codes, who wished to exchange new ideas, methods and results, in an informal setting. By no means was this meeting intended to conflict with the Ninth Conference on Numerical Simulation of Plasmas scheduled for June 30 - July 2, 1980 at Northwestern University, sponsored by Professors J. Denavit and G. Knorr, which covers a much wider area and is to be published.

Lastly, the particle-hybrid code community had concern that the very real contributions of particle and particle-fluid simualtions to the understanding of fusion plasmas, in support of both theory and experiment, might just have been underestimated in Washington. This conference is, in part, a reaction to recommendations of the DOE committee for computer time allocations for FY80 which included: major labs receiving 63% of their requests, but universities receiving only 40%; the decision that large particle pushing or kinetic codes can be afforded only sparingly; basic plasma theory was given approximately a 20% absolute cut; ability to follow out unexpected results was cut to a bare minimum; studies of alternate concepts were cut more than were mainline studies. The challenges to the community are clear: make our contributions known; make our codes more efficient in terms of useful physics per unit of computer time (optimize, use minimum number of dimensions and particles, etc.); check code physics by

analysis (time and spatial grid effects, fluctuations) and by comparison with known linear and nonlinear results so as to increase confidence in the simulations.

Editorially we note that the field has matured considerably from the early desk calculator work of Buneman and Hartree on magnetrons in the early 1940's, the one dimensional electrostatic plasma work on modern computers by Buneman and Dawson in the late 1950's, to the current 2d and 3d fully electromagnetic codes of Langdon, Buneman and others. The early science has become more of an art. Simulation for magnetic fusion has now become strongly applications oriented, with DOE devoting the bulk of FY80 computing resources to the direct support of existing experiments and the design of next generation devices, including calculations of transport, impurities, heating, stability, equilibrium, coil design, etc., a milestone indeed. Coupled with this new emphasis is the current plateau in large computer time for magnetic fusion, with no relief planned until at least summer 1981. These factors present a challenge to all of us to be more efficient and more effective in our simulations.

Co-ordinators: C. K. (Ned) Birdsall Alex Friedman
U. C. Berkeley, December 17, 1979

II. SCHEDULE

Final Schedule for
Informal Conference on Particle and Hybrid Codes for Fusion
December 10-11, 1979, Napa, California

- -

Conference coordinated by Charles K. (Ned) Birdsall, Alex Friedman, assisted by Ginger Pletcher, at the Electrical Engineering and Computer Science Department, University of California, Berkeley 94720

There will be four main sessions. Talks will be 20, 15 and 10 minutes with adequate time for discussion. If certain subjects draw great interest, additional time will be available.

Of general interest is the efficiency of particle and particle-fluid codes, in terms of physics output per unit of computer resource (time, memory, volume of output, etc.). Of comparable interest is the progress toward working at lower and lower frequencies, with larger mass ratios, etc.

MONDAY, DECEMBER 10
Session IA - 8:30 am to 12:00 noon Chairperson: C. Nielson

* Long-time-averaging (LTA). Particle simulation of slow transport phenomena.
* Particle MHD vis a vis fluid MHD and other fluid codes.
* Large time step problems (mi/me>>1, omega dt>>1, digital filtering, stiff equation integrators).

*Paper numbers here correspond to paper numbers in the proceedings' book, which was sent to all participants.

Session IB - 1:30 pm to 5:00 pm Chairperson: C. K. Birdsall

* David Nelson; view from DOE.
* Improvements in simulation 1974 to 1979, and future.
* Code production vs development running times; allocations and priorities.
* Hardware, e.g. array processors, graphics, class VII computers.
* Efficient 3d simulation; 3d grid vs 2d+Fourier representation.

C. K. Birdsall, Comments on 1974 Berkeley Meeting; hopes for this meeting.

TUESDAY, DECEMBER 11

Session IIA - 8:30 am to 12:00 noon Chairperson: J. Denavit

* Linearized codes.
*Modified particle codes (use of linear susceptibility or Boltzmann response, 1d stretched to 2d or 3d).
* Quasineutral, hybrid, and Darwin codes (applications to confinement, compression, equilibrium, stability, and transport).
* Buildup and plasma trapping, neutral beam injection, and wave heating (laser-pellet plasmas, pinches, mirrors, tokamaks).

Session IIB - 1:30 pm to 4:00 pm Chairperson: O. Buneman

* Inhomogeneous plasmas (fluctuations, initialization techniques in 2d and 3d).
* Undesirable instabilities in warm plasma simulations (e.g. multi-beam and multi-ring).
* Grid effects (e.g. curvilinear coordinators, div B nonzero).

4:00 pm to 5:00 pm Moderator: B. Cohen

* Panel Discussion: When to use a particle, fluid, or hybrid code (on none at all). All participants invited to contribute.

Panelist: J. Denavit, A. B. Langdon, B. McNamara, C. Nielson, H. Okuda

III. PANEL DISCUSSION*

(B. Cohen, moderator: J. Denavit, A. B. Langdon, B. McNamara, C. Nielson, H. Okuda)

Plasma simulation is one tool in the attack on understanding plasmas which will eventually result in the design of fusion reactors. Simulation using thousands of particles vies for usefulness with simulation using a few fluids. Particle codes can deliver the full kinetic behavior, which is sometimes needed; fluid codes use parameters from theory, particle simulation, and/or experiment, and deliver average or long-term information. Particle-fluid hybrids attempt to use the best features of both, mixing fast and slow time scales.

Particle codes, in some quarters, have gained a reputation for using more computer time per unit of useful physics than used by fluid codes. This reputation is considered undeserved by those particle simulators who work with limited budgets, use the least number of dimensions for the problem at hand, use the least number of particles necessary, and use hybrid simulation where applicable. However, there appears to be room for further optimization. Those with larger computing budgets, please follow.

Okuda addressed the progress made in understanding anomalous transport indigenous to tokamaks, moving from an early fully dynamic (hence, expensive) model to guiding center electron models in 3d, both electrostatic and magnetostatic, with long time steps (less expensive), toward a 3d toroidal model for steady state, including turbulence and transport, poloidal divertors, and hybrid heating. These models are particularly useful for

*This section was written from my notes and has been checked over by the panelists (C. K. Birdsall).

low β plasmas. He also gave an example in which the low frequency ion acoustic instability can drive the high frequency two-stream instability unstable by nonlinear effects; this is a warning that the long-time-step, time-averaged low frequency method may break down for certain plasma parameters. Whether or not this kind of process can occur for other low frequency instabilities is not known. In any case, one must be extremely cautious when modeling low frequency phenomena by discarding high frequency responses since they can make a large change in what one is looking for.

Denavit observed that hybrid codes, 3d particle codes, with time filtering, long time scales, all appear to be problem dependent. In conflict with this, there is the need for optimization via assembly language, which implies loss of flexibility. We are fortunate, in particle simulation, to be able to work on interesting problems and to obtain useful results. Simulation identifies physical mechanisms, suggests theoretical work and rejects ideas that do not fit.

Nielsen stated that simulation must continue in order to keep theorists honest; simulation is the only economical means of checking theory directly open to them. The question is not whether, but how to continue, effectively. We must pay more attention to macroscopic work; as we do, we are likely to find that distinctions between particle and fluid work will disappear. The new hardware is revolutionary, but there still is an open question as to using one big computer or many small machines; his view is that special computers are still too small, too complicated to use.

McNamara presented a list of unresolved problems as follows:

Tokamaks

1. Anomalous electron transport
   — is it really classical?
2. Nonlinear effects of ballooning and tearing

Field Reversal

1. Non-axisymmetric states in RFP
2. Equilibria and stability of large orbit FRM

Tandem Mirrors

1. Nonlinear saturation of cyclotron modes
2. MHD stability and ballooning
3. Energy transport in tandems, thermal barriers, etc.

His upbeat view is as follows:

1. Simulation is very effective and increasingly realistic. Therefore, push major design and physics efforts for fusion systems.
2. Provide more software and graphics support for designated activities. Others benefit by fallout.
3. Encourage more collaboration — from three day advisory groups for new problems to joint efforts and publications.
4. Improve the numerical analysis input — without a $200K tax to pay for it.
5. Write more reviews on the state of the art and advertise good results more vigorously.
6. Long term goals — Design a fusion reactor: Are we getting there?

McNamara also presented a chart, computational attack on plasma parameters, as attached. Note the marriages of all kinds, across fuzzy boundaries, particle plus fluid; micro plus macro; dynamics plus equilibria, etc. McNamara ended by repeating the need for more advertising of accomplishments.

THE COMPUTATIONAL ATTACK ON PLASMA PARAMETERS

(B. McNamara)

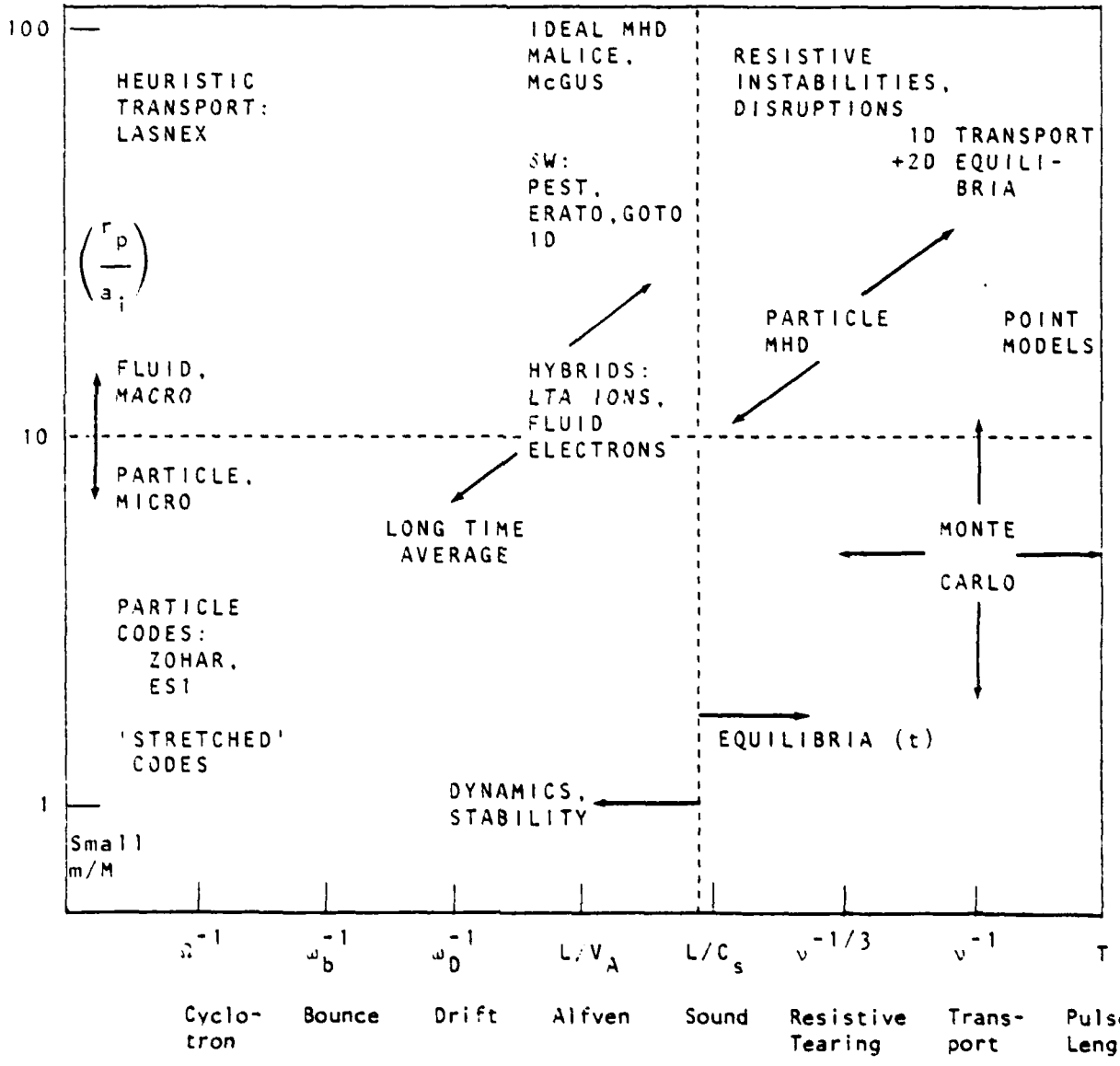

Langdon noted that the MFE computational effect has grown greatly in the last five years. He repeated his advice of the 1974 meeting that, if we want to work with long time scales, implicit time integrations will be required which may not be attractive, but are needed, because explicit methods will end up unstable at large $\omega\Delta t$. He suggests turning to continuum methods for modeling kinetic physics - painful, but needed (Rod Mason has done some, with multigroup transport). He is interested in partially kinetic models.

Cohen concluded the panel discussion with the observations that scaled variables will probably always be with us, that having computer variables match experiment is probably impossible in the foreseeable future. He presented a summary chart on hybrid simulations, attached. His work and that of others, has moved particle simulation into physics on transport time scales.

Birdsall sketched on the blackboard the DOE hierarchy of models, with increasing expense (reading left to right),

ideal multifluid drift-kinetic hybrid Maxwell-Boltzmann single particle

and his interactive model

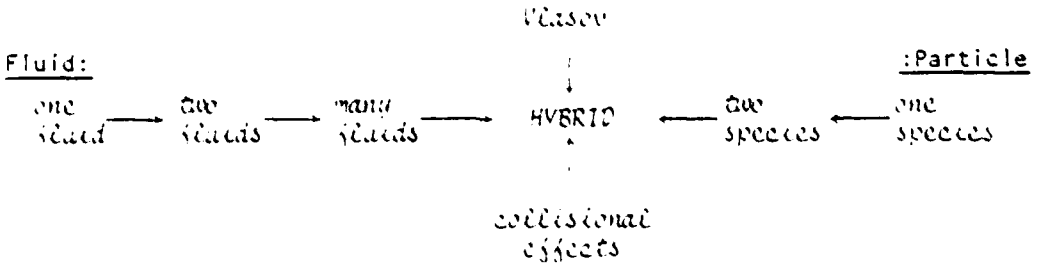

making the point that these models interact, are mutually supportive, and are seldom wholly independent; over-emphasizing one tool or removing another might well reduce the efectiveness of the remaining system.

HYBRID SIMULATIONS - PHILOSOPHY

(B. Cohen)

Kinetic detail requires particles [or $f(\vec{v})$ description]

$a_s/R_p = \mathcal{O}(1\pm)$	large-orbit equilibrium & transport, e.g., field reversal; $a_s \equiv v_{\perp s}/\omega_{cs}$
$a_s/\lambda_{wave} = \mathcal{O}(1\pm)$	microinstability, e.g., drift waves
$\lambda_D/L_n = \mathcal{O}(1\pm)$	sheaths
$\omega - k_\parallel v_\parallel + \ell\langle\omega_{ci}\rangle + p\omega_{bounce} = 0$	Landau resonance, e.g., wave (±) dissipation, trapping, overlap of resonance

When kinetic detail is *un*necessary, elimination of particles and fine time & space scales and adoption of fluid description can greatly extend computational power. $m_e/m_i \ll 1$ often separates ions & electrons.

ω/ω_{cs} , $a_s/R_p \ll 1$	drift approximation
ω/ω_{cs} , $a_s/R_p \gg 1$	unmagnetized, straight-line orbits
$\langle v\rangle \ll \omega/k$	hydrostatic
$\langle v\rangle \gg \omega/k$	adiabatic
linear phenomena	linear dielectric, $\chi_s(\omega \sim i\partial_t, k)$

Payoff: Analytic reduction of fluid description, appropriate to specific parameter regimes and problems, (1) result in large savings of computer memory & time, and (2) greatly extend the range of parameters accessible to simulation.

Directions:

1. Simulation of transport with hybrid orbit-averaged code
2. Hybrid simulation of microinstabilities with more realistic parameters and geometries.

IV. CONCLUSIONS

(from C. K. Birdsall's notes)

Many of these are already in the Panel Discussion.

The 1974 conference, for the same purposes, covered a number of topics which are now pretty well resolved, e.g., particle weighting battles are mostly past, with linear and quadratic weighting widely used and understood (multipole use isolated); hybrid codes were just starting then and now exist in a variety of forms; 3d codes, then done by one or two groups only are now done by several; one special purpose computer was mentioned then, with many now.

However, several authors from 1974 gave up-dates in 1979 on problems still not fully resolved, such as linearized particle codes, long-time-scale particle simulations, the plea for use of implicit schemes for large time steps, and 3d economical codes. The 1974 conference called for more use of hybrids (happening), more emphasis on simulations including inhomogeneous density, magnetic field, temperature, etc. (happening) and for honest use of two species, large m_i/m_e (happening somewhat). Perhaps the long-term needed to resolve these problem areas indicates their toughness and rasies the question of pursuing them further - some of them obviously must be.

David Nelson's view from DOE, paper #10, was provocative. The loud and clear messages were that magnetic fusion computing capability is fixed, with no relief expected before 1981, with increasing allocations to device specifics and less to large particle pushing or kinetic codes. His list of problem areas needing more attention from particle simulators was:

Divertors, axi- + non-axi-symmetric sheaths, potentials, boundary layers, ambipolarity,

Plasma edge including shadow of limiter, neutrals, atomic physics, reflux, metal surface,

Transport in non-axisymmetric systems,

RF heating including nonlinear effects

Optimization of gyrotron geometry

Stability of EBT ring-plasma

Formation + tearing problems in RFM, RFΘP, spheromak

All the old unsolved problems including bump on tail (α particles).

Nelson's cost-hierarchy of models, repeated at the end of the panel discussion write-up, was intended to persuade simulators to seek the most appropriate model, matched to the physics sought, using the simplest (least expensive) first and then, if need be, moving on to more elaborate (more expensive) later. This ranking was not intended as some form of cost-effectiveness argument for and against fluid versus particle simulations.

Bruce Langdon, in Paper #11, made several strong suggestions about doing MFE computing more effectively and more efficiently. Optimization pays off very quickly (he gave experience with ZOHAR showing that optimization paid off almost as it was done!) Optimization must be done selectively, so as not to hurt in making changes (e.g., ZOHAR particle boundary conditions are handled in Fortran). He advocated: use of monitoring, intervening, postprocessing, and linking to other codes; relying heavily on interactive codes, sharing the (large) data set of the simulation code, doing considerable computing and driving rapid graphic displays. Postprocessing is very helpful in evoking good physical understanding, such as spectra, filtering, finding spatial and temporal correlations, etc. Fast graphic display, like LLL's TMDS, is extremely valuable. The pitch to MFE was not only to update software, but also to update hardware.

V. RECOMMENDATIONS
(from C. K. Birdsall's notes)

Recommendations are both explicit and implicit in the Panel Discussion and in the above. *TO ALL:*

(1) in computing be more effective, more efficient;

(2) in physics, make results better known.

TO DOE:

(1) be more aware of the day-by-day interactions within the particle simulation-theory-experiment net, continually refining theory and fluid codes;

(2) be more aware that most particle simulation workers have moved toward particle-fluid models to stay;

(3) note that particle simulations are now capable of working on transport time scales;

(4) plug, on your end, for more efficient equipment;

(5) include particle simulation people on your computer time allocations committee;

(6) reward inventions, like long-time averaging, orbit-averaging, hybrid codes, MHD-particle codes, use of global integrals of motion, use of macrocells, etc., when these result in real savings;

(7) keep alive support of the smaller university efforts, which in turn aid much in keeping honest the larger national lab efforts;

(8) penalize users with larger budgets who are slow to use new invention to save time;

(9) do away with "if you don't use it, you lose it" budget policy.

DISTRIBUTION LIST - 1

Department of Energy
Manley, Nelson, Price, Priester, Sadowsky, Siambis

Department of Navy
Condell

Austin Research Associates
Drummond, Moore

Bell Telephone Laboratories
Hasegawa

Calif. State Ploytech. Univ.
Rathman

Columbia University
Chu

Cornell University
Mankofsky

Electrical Power Research Inst.
Gough, Scott

General Atomic Company
Helton, Lee

Georgia Institute of Technology
Bateman

Hascom Air Force Base
Rubin

IBM Corporation
Gazdag

JAYCOR
Klein, Tumalillo

Dory, Meier, Mook

Princeton Plasma Physics Lab.
Chen, Cheng, Lee, Okuda, Tang

Princeton University
Graydon

Science Applications, Inc.
McBride, Wagner

Sandia Laboratories
Freeman, Poukey, Quintenz

Stevens Institute
Rosen

Sonoma State University
Johnston

Stanford University
Buneman

University of Arizona
Morse

Univ. of California, Berkeley
Arons, Au-Yeung, Birdsall, Buchanan, Chen, Chorin, Friedman, Grisham, Harned, Hudson, Keith, Kim, Lichtenberg, Lieberman, McKee, Otani, Potter, Thomas

University of California, Davis
DeGroot, Woo

University of California, Irvine
Rynn

Univ. of Calif., Los Angeles
Dawson, Decyk, Huff, Liewer, Lin, Tajima

DISTRIBUTION LIST - 2

Air Force Base
Genoni, Pettus

Los Alamos Scientific Laboratory
Barnes, Burnett, Forslund, Gitomer, Hewett, Lewis, Lindemuth, Lindman, Mason, Neilson, Oliphant, Sgro

Lawrence Berkeley Laboratory
Cooper, Feder, Kaufman, Kunkel, Pyle

Lawrence Livermore Laboratory
Albritton, Anderson, Brengle, Briggs, Bruijnes, Byers, Chambers, Cohen, Condit, Estabrook, Fawley, Finan, Fries, Fuss, Harte, Killeen, Kruer, Langdon, Lasinski, Lee, Maron, Marx, Matsuda, Max, McNamara, Mirin, Nevins, Nielson, Smith, Tull

Mass. Institute of Technology
Berman, Bers, Gerver, Kulp, Palevsky, Tetreault

Mission Research Corporation
Hobbs, Godfrey

NASA - Langley Research Center
Hohl

U.S. Naval Research Laboratory
Boris, Drobot, Haber, Orens, Vomvoridis, Winsor

Northwestern University
Crystal, Denavit

New York University
Grad, Weitzner

Oak Ridge National Laboratory

University of Iowa
Joyce, Knorr, Nicholson

University of Maryland
Guillory, Rowland, Sternlieb, Winske

University of Texas
Horton, MacMahon

University of Wisconsin
Shohet

Culham Laboratory
Eastwood, Roberts

University of Reading
Hockney

Ecole Polytechnique / Centre de Polytech.
Adam

Bhabha Atomic Research Centre
Aiyer

Gell

Tel-Aviv University
Cuperman

Nagoya University
Kamimura

Max Planck Inst. fur Plasmaphysik
Biskamp